University of South-Eastern Norway
Faculty of Technology, Natural Sciences and Maritime Sciences

Master's Thesis

Study programme: Master of Science in Micro and Nano Systems Technology

Spring 2023

Farshad Farahi Bolamiri

Numerical simulation of microplastics trapping in a microfluidic channel utilizing travelling acoustic waves

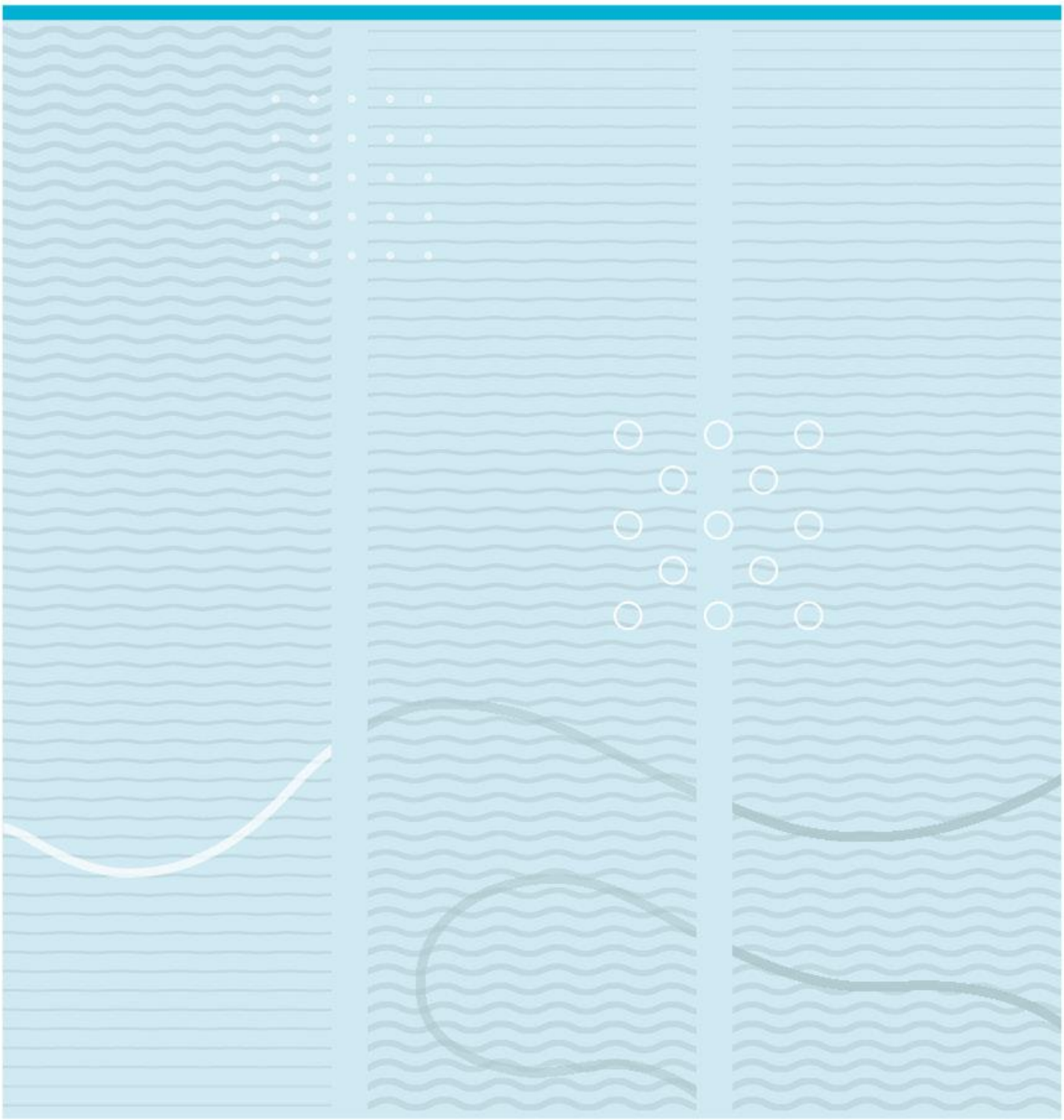

University of South-Eastern Norway
Faculty of Technology, Natural Sciences and Maritime Sciences
Department of Microsystems.
Raveien 215
NO-3184 Borre, Norway

http://www.usn.no

Summary

A numerical simulation based on a novel acoustofluidics model with travelling surface acoustic waves has been provided. An acoustic radiation force equation from travelling acoustic waves has been introduced to COMSOL Multiphysics finite element model software. This new model has been validated through an example and characterized by simulating microparticles trajectories through changing the size and density of microparticles as well as driving conditions such as normal inflow velocity of microchannel, voltage, and frequency of travelling surface acoustic waves resonator. This model can be used to trap microplastics on top of a microchannel in order to quantify them in a sample.

Acoustic radiation force has been discussed analytically and some important simulation results of acoustic fields such as total acoustic pressure and velocity as well as stationary field of velocity magnitude of laminar flow in microchannel have been provided. These results are used to simulate microplastics trajectories in the microchannel. In describing the modelling process in COMSOL, it is tried to be written like a tutorial so that it could be useful for those who are interested in modelling acoustofluidics domains.

Simulation results show that by choosing appropriate design parameters such as microchannel flow rate, voltage, and frequency of surface acoustic wave resonator, microplastics with diameters bigger than 7 μm and density of 950 kg/m^3 can be trapped on the ceiling of microchannel above the resonator.

Preface

I would like to express my sincere gratitude to my supervisors, Associate professor Hamed Salmani, Professor Ulrik Hanke, and Associate professor Agne Johannessen at University of south-Eastern Norway. Their insights and expertise helped me to shape the direction of my work and achieve the goals of this project.

I am grateful to my family for their unwavering supports and encouragements during my studies. Their love and encouragement kept me motivated and focused.

I would like to acknowledge Centre for Sustainable Transition at University of south-Eastern Norway for providing financial support for my research. I would also like to thank RFF Vestfold og Telemark for supporting us with the project number 337766. Their funding has made a valuable contribution to my master thesis.

Thank you to everyone who has helped me in any way during my research journey. Your contributions have been invaluable and will never be forgotten.

3184 Borre, Norway, May 20, 2023

Farshad Farahi Bolamiri

Contents

1 Introduction

The flow of fluids in a channel with sub-millimeter-sized cross section is called microfluidics [1]. Laminar flow in microfluidics paves the way for applying controlled force on the particles in order to handle them based on different physical properties such as inertia, electrokinetics, dielectrophoretics, magnetophoretics and mechanical contact forces [1]. These techniques have been used to address some challenges in handling biological targets such as blood cells [2].

Acoustofluidics that is the technology of employing acoustic waves in microfluidic, is a rapidly growing technique to handle micro and nanoparticles in biology, medicine, chemistry, engineering, and physics [2]. It is a biocompatible and label free approach for handling biological targets based on their mechanical properties such as size and density, regardless of some of their physical properties such as electric or magnetic ones [3]. For instance, this technique has been used to separate blood cells from plasma as well as exosomes from whole blood with purity of more than 98 percent [2].

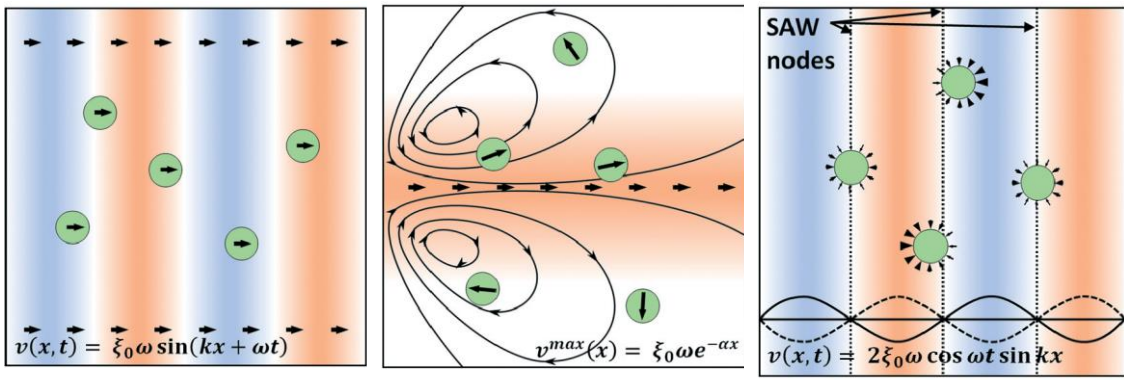

(a) *(b)* *(c)*

Figure 1-1 Three most commonly used acoustofluidics technique for manipulating microparticles through (a) acoustic travelling wave, direction of particles displacement is parallel to the wave vector of travelling wave, (b) acoustic streaming where particles follow streamlines by Stokes drag force, and (c) acoustic standing waves where particles are accumulated on nodal lines. $\boldsymbol{v(x,t)}$ *shows velocity amplitude of substrate for a surface acoustic wave (SAW), where* $\xi_0\omega$ *is the velocity amplitude and k and* ω *are wave number and angular frequency, respectively* [4].

Figure 1-1 shows three most commonly used acoustofluidics techniques by which microparticles can be translated [4]. In Figure 1-1 (a), particles are pushed along the direction of acoustic travelling waves by means of acoustic radiation force while in Figure 1-1 (b), they follow acoustic streamlines. In Figure 1-1 (c) microparticles tend to displace towards nodal lines in a standing acoustic field where pressure and acoustic radiation force are zero.

Regarding acoustofluidics separation techniques, both standing and travelling surface acoustic waves enjoy high precision separation and are easy to miniaturized, however, they suffer from low throughput [2]. Moreover, standing surface acoustic waves can exert stronger acoustic radiation force on particles compared to travelling one but it needs usually more than one interdigitated transducer (IDT) [2].

1.1 Acoustofluidics in the Literature

After the early success in segregating microparticles in on-chip acoustophoretic devices, this technique was employed in different biotechnical applications such as cell trapping, plasmapheresis, forensic analysis, food analysis, cell sorting using surface acoustic waves, cell synchronization, and cell differentiation [1].

1.1.1 Experimental work

Most of the acoustofluidics separation technique reported experimentally in the papers have been implemented by means of standing surface acoustic waves (SSAW) or travelling surface acoustic waves (TSAW). Ding et al. [3] introduced a tilted-angle standing surface acoustic waves (taSSAW) where these waves make an optimized angle with flow direction in the microchannel. They reported separation of 2 and 10 µm Polystyrene beads with an efficiency of almost 99%. This method can be used to separate MCF-7 breast cancer cells from white blood cells.

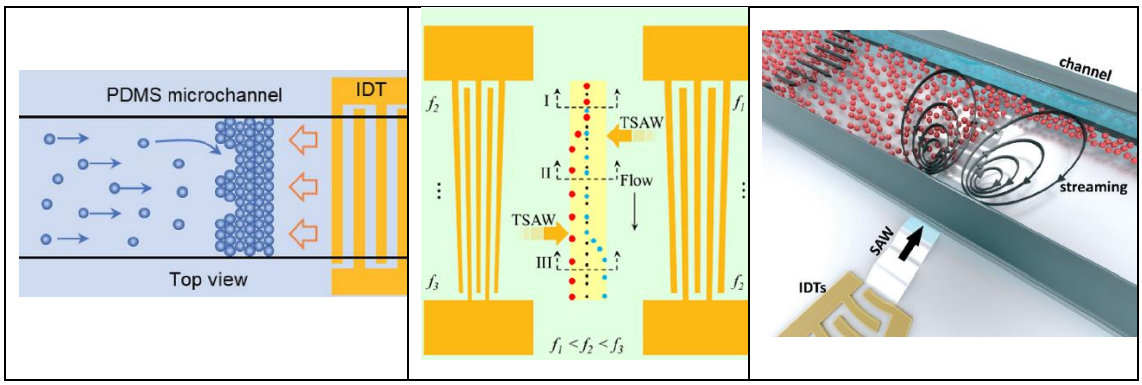

(a) *(b)* *(c)*

Figure 1-2 travelling surface acoustic waves separation technique with three different interdigitated (IDT) electrodes structures of (a) uniformly spaced [5], (b) slanted interdigitated transducer (SIDT) [6], and (c) focused electrodes [4]

Travelling surface acoustic waves separation methods can be categorized by the configuration of interdigitated transducer (IDT) that is employed to convert electrical energy into acoustical one in form of Rayleigh waves [7]. Destgeer et al. [5] employed an IDT with uniformly spaced electrodes to push 10 µm Polystyrene beads to the ceiling of a microchannel at frequency of 72 MHz. This technique can be used in the self-assembly process where any cracks and defects in the lattice structure can be filled with microparticles, see Figure 1-2(a). In another work, Destgeer et al. [6] utilized a slanted interdigitated transducer (SIDT) to generate tunable travelling surface acoustic waves with three different frequencies $f_1 < f_2 < f_3$ to deflect three particles with different size in a hydrodynamically focused sample fluid, see Figure 1-2(b). Their design enjoys anechoic corners where acoustic radiation force cannot affect particles located in the microchannel corners. Collins et al. [4] have employed a resonator producing high frequency focused surface acoustic wave in order to displace submicron particles, which are hardly affected by acoustic radiation force[8], through utilizing both acoustic radiation force and streaming[4], see Figure 1-2(c). The IDT comprises circularly focused electrodes with frequency of 633 MHz that can focus 100, 300, and 500 nm particles.

1.1.2 Modelling and numerical simulations

Acoustic radiation force (ARF) and Stokes drag force arising from oscillatory and steady acoustic fields play a prominent role in defining trajectories of microparticles in a microfluid. Since measuring these two forces is difficult through experiments, numerical model not only can be used to calculate these forces, it can also simulate particles trajectories [7]. Moreover, with the recent advancement in computerized calculations and availability of user-friendly finite element software, the interest in providing a fully coupled numerical simulation of acoustofluidics, that can accurately predict the behaviour of microparticles in such medium, has been increased. For example, Hahn et al. [9] have provided a platform for 3D trajectory simulation that can simulate radiation force and hydrodynamic drag on particles with different shape, size and structure. The proposed model, firstly, simulates the time-harmonic acoustic fields to drive acoustic streaming field and acoustic radiation force. The drag and coupling coefficient are also derived by hydrodynamic simulation. The results of these simulation in COMSOL are given to MATLAB to drive the particle velocity in time domain and consequently its position. Although they could propose a 3D model having the ability to simulate both translational and rotational trajectories of particles that are not spherical and homogenous, the proposed platform is restricted to bulk acoustic wave (BAW) devices and the simulation is not integrated in just one software. Trying for providing a numerical model of acoustofluidics utilizing standing surface acoustic waves (SSAWs), Namnabat et al. [10] have provided a comprehensive numerical simulation of boundary-driven acoustic streaming by the limiting velocity finite element model. They introduced acoustic radiation force formula to COMSOL and validated the model by comparing the Polystyrene beads trajectories from the simulation with one reported experimentally. Regarding recent works in modelling acoustofluidics devices, Wang et al. [7] have compared conventional structure of SAW-PDMS with hybrid structures of SAW-glass, SAW-SAW, and SAW-PZT, see Figure 1-3 [7]. They have compared these four structures in terms of manipulation time and percentage of particles accumulated on nodal points for microparticles with diameter of 1 μm,5 μm, and 10 μm. The comparison shows that both hybrid structures of SAW-SAW and SAW-PZT have better performance in accumulating more particles in shorter time than the other two structures.

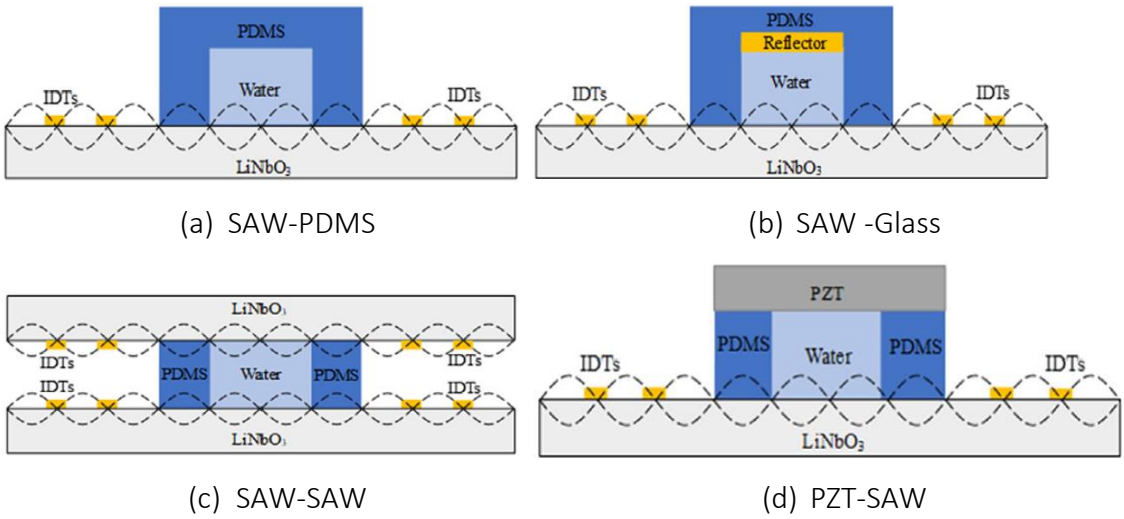

Figure 1-3 four different acoustofluidics structures (a) conventional structure with SAW resonator and PDMS microchannel, (b) SAW resonator with glass as reflector at other side of microchannel, (c) employing two SAW resonator at top and bottom sides of microchannel, and (d) SAW resonator with PZT on top of PDMS microchannel [7]

1.2 Numerical simulation of acoustofluidics utilizing TSAWs

Deflecting and trapping Polystyrene particles, for example, through utilizing travelling surface acoustic waves in acoustofluidics devices have been reported experimentally in literatures [6], [5], [11]. However, there is a lack of numerical simulation on particles trajectories arising from acoustic radiation force of travelling waves.

In this master thesis, a novel platform for simulating acoustofluidics devices utilizing travelling surface acoustic waves in COMSOL finite element model software has been provided. In the proposed model, acoustic fields of pressure and velocity arising from travelling waves in frequency domain as well as stationary fields of drag force and acoustic streaming are simulated and used to calculate acoustic radiation force. Since the simulations has been carried out during implementing this model showed that the available equation in COMSOL for acoustic radiation force cannot be used to simulate particles trajectory arising from acoustic travelling wave accurately, a new permissible equation for calculating such force which is described by Settnes and Bruus in [12], has been introduced to COMSOL instead of its main equation. This model has been validated

by comparing the simulated acoustic radiation force with an example described in [12]. Finally, the model has been characterized through evaluating effect of changes in driving condition like voltage and frequency of TSAW resonator as well as size and density of particles on particle trajectories.

1.3 Microplastics manipulation by acoustofluidics

Microplastics (MPs) are considered as one of the main issues threatening human life and other creatures on the earth nowadays [13]. The adverse effects of these particles, that are less than 5mm in diameter [14], have been recently highlighted not only in scientific papers but also in the media. MPs that lie at the root of low degradation of unsustainable materials used by humans [15]–[17], are existing now in different ecosystems from land to oceans [13]. This worldwide problem has been addressed in the UN SDGs, Sustainable Development Goals, particularly Goal 14 which is to: Conserve and sustainably use the oceans, seas, and marine resources for sustainable development [5]. Without any doubt, one of the most important ways in terms of transition to a more sustainable world is to remove environmental footprint of unsustainable materials like plastics. Dealing with this problem is especially of importance for countries like Norway enjoying long coastlines.

The first important step in overcoming this issue is to continuously quantifying MPs in an ecosystem, particularly in this case, aquatic environment. The most commonly applied technique for measuring the number of MPs is optical microscopy which can suffer from being laborious [18].

The proposed model can be used to address this issue where microplastics can be trapped on the ceiling of microchannel in order to be quantified. Figure 1-4 shows a 3D and cross-sectional schematic diagram of the proposed model comprised of a rectangular microchannel and travelling surface acoustic waves (TSAWs) resonator for trapping and consequently quantifying microplastics particles. In this Figure, TSAWs are generated by piezoelectric interdigitated transducer (IDT) so that the acoustic radiation force is equal to opposing Stokes drag force to concentrate particles[5].

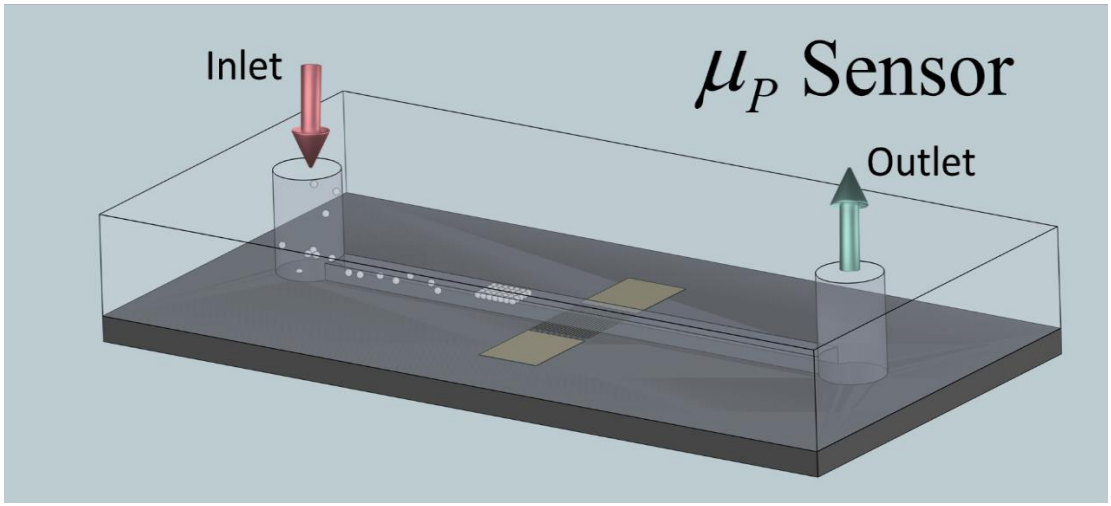

(a)

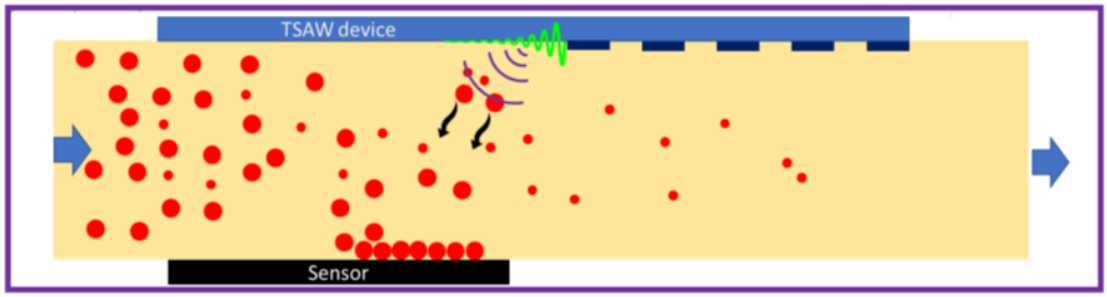

(b)

Figure 1-4 3D and 2D cross-sectional schematic diagrams of the proposed model comprises TSAW resonator at one side of rectangular microchannel to push MPs (white in (a) 3D &(b) red in 2D) on the surface of a sensor placed at the other side in order to quantify these particles.

One of the main advantages of the proposed cost-effective model compared to microscopy technique is the ability to do real-time and on-site measurement at temporary lab or automatic measurement in subsea robots, for instance.

1.4 The structure of thesis

Most of the equations and relations provided in this thesis come from lab on a chip tutorial series on acoustofluidics written by a group of researchers to explain the state of art acoustofluidics technology for students and researchers [19].

Chapter 2 and 3 introduce some of governing equations of microfluidics and acoustofluidics including mathematical notation used throughout this thesis, some flow solutions based on Navier-Stokes equation and perturbation theory. Chapter 4 deals with acoustic radiation force and streaming in microfluid which determine microplastics trajectories. In chapter 5, the steps of modelling process in COMSOL are given in details followed by some important simulation results which are used in calculating two main forces of acoustic radiation force and Stokes drag force. chapter 6 deals with the equation of acoustic radiation force introduced to COMSOL with simulation of MPs trajectories with characterization of the proposed acoustofluidics model. A list of variables and expression which are used for simulating the proposed model in COMSOL are given in appendix.

2 Microfluidics and the governing equations

The laminar flow of a fluid in a microchannel provides a platform for manipulating microparticles that has been extensively used in separating biological samples [2]. Therefore, understanding the governing equations of microfluidics is necessary for analyzing acoustofluidics models. This chapter starts with introducing some mathematical notations and definitions, followed by some basic and governing equations in microfluidics formulated based on classical continuum field of velocity $\boldsymbol{v}$, pressure p, and density ρ [1]. More details on the basic continuum fields and how to derive microfluidics governing equations are presented by Bruss [1], [20]. At the end, some basic flow solutions are shown.

2.1 Mathematical notation

Due to the non-linear nature of partial differential equations governing microfluidics, dealing with them can be complicated [1]. For simplification, some notations are presented based on the reference [20, p. 7].

Firstly, Cartesian co-ordinate system (x, y, z) with corresponding basic and mutually orthogonal vectors $\boldsymbol{e_x}, \boldsymbol{e_y}$, and $\boldsymbol{e_z}$ is used to derive the equations. The position vector, $\boldsymbol{r} = (r_x, r_y, r_z) = (x, y, z)$ is written as:

$$\boldsymbol{r} = r_x\boldsymbol{e_x} + r_y\boldsymbol{e_y} + r_z\boldsymbol{e_z} = x\boldsymbol{e_x} + y\boldsymbol{e_y} + z\boldsymbol{e_z}. \qquad (2\text{-}1)$$

To present a vector $\boldsymbol{v}$ by its components v_i(for Cartesian coordinate$i = x, y, z$), Einstein summation convention is used as below:

$$\boldsymbol{v} = \sum_{i=x,y,z} v_i e_i \equiv v_i e_i \ . \qquad (2\text{-}2)$$

Regarding partial derivatives, the symbols ∂_i, with $i = x, y, z$ and $\partial_t$are used for a given function $F(x, y)$:

$$\partial_x F \equiv \frac{\partial F}{\partial x},\ and \quad \partial_t F \equiv \frac{\partial F}{\partial t}. \tag{2-3}$$

The vector differential operator nabla ∇ is defined as:

$$\nabla \equiv e_x \partial_x + e_y \partial_y + e_z \partial_z = e_i \partial_i. \tag{2-4}$$

Regarding the nabla operator, Laplace operator can now be defined as:

$$\nabla . \nabla \equiv \nabla^2 = \partial_i \partial_i. \tag{2-5}$$

The divergence of a vector field $\boldsymbol{v}$ is:

$$\nabla . \boldsymbol{v} \equiv \partial_x v_x + \partial_y v_y + \partial_z v_z = \partial_i v_i. \tag{2-6}$$

Note that $\nabla . \boldsymbol{v}$ is different from $\boldsymbol{v} . \nabla$, former is a scalar function whereas the latter is a scalar differential operator [1].

2.2 Governing equations

2.2.1 The continuity equation

The first equation to be discussed is the continuity equation that is based on the conservation of mass [1]. By considering a compressible fluid where the density ρ can be changed according to space and time, and assuming a fixed, arbitrary shaped region Ω in the fluid, it is shown that [1]:

$$\partial_t \rho = -\nabla . (\rho \boldsymbol{v}) \quad or \quad \partial_t \rho = -\partial_j \left(\rho v_j\right). \tag{2-7}$$

where $\boldsymbol{v}$ is the velocity field.

In microfluidics, density ρ can be considered constant, i.e., incompressible fluid[1], so the continuity equation becomes:

$$\nabla . \boldsymbol{v} = \partial_i v_i = 0. \qquad (2\text{-}8)$$

2.2.2 The Navier-Stokes equation

The second governing equation that is related to momentum conservation and the momentum density ρv as well as derived based on the conservation of mass [1], is the well-known Navier-Stokes equation. The derivation process can be found in several references like [1], [20].

Navier-Stokes equation for compressible fluid can be written as:

$$\rho[\partial_t \boldsymbol{v} + (\boldsymbol{v}.\nabla)\boldsymbol{v}] = -\nabla p + \eta\nabla^2\boldsymbol{v} + \beta\eta\nabla(\nabla.\boldsymbol{v}) + \rho g. \qquad (2\text{-}9)$$

where $\boldsymbol{g}$ is the gravitational acceleration. The viscosity coefficients $\boldsymbol{\eta}$ and $\boldsymbol{\beta}$ can be considered constant at a given temperature for a Newtonian fluid [1].

For incompressible fluid where the divergence of velocity equals zero, equation (2-9) becomes,

$$\rho[\partial_t \boldsymbol{v} + (\boldsymbol{v}.\nabla)\boldsymbol{v}] = -\nabla p + \eta\nabla^2\boldsymbol{v} + \rho g. \qquad (2\text{-}10)$$

Finding analytical solution for the non-linear Navier-Stokes equation seems difficult, however, for small flow velocities, it can be rewritten in linear form [1]. Reynold's number $\boldsymbol{Re}$ is defined to determine the condition for neglecting non-linear term.

$$Re \equiv \frac{\rho V_0 L_0}{\eta}. \qquad (2\text{-}11)$$

For instance, Reynold's number is calculated by Bruss [1] for typical values of $\eta/\rho = 10^{-6} m^2 s^{-1}$, $L_0 \approx 10^{-4} m$, and $V_0 \approx 10^{-3} m s^{-1}$ that is $Re \approx 0.1$ for water. For $Re \ll 1$, the non-linear Navier-Stokes equation is simplified to the linear equation [1],

$$\rho\partial_t \boldsymbol{v} = -\nabla p + \eta\nabla^2\boldsymbol{v} \qquad (2\text{-}12)$$

For a constant pressure through channel, it can be rewritten as a diffusion equation [1],

$\partial_t v = \vartheta \nabla^2 \boldsymbol{v}$, with $\vartheta = \frac{\eta}{\rho}$ (2-13)

where, ϑ is called the kinematic viscosity and define the diffusivity of momentum in the fluid [1].

2.3 Flow solutions

There are some analytical solutions for Navier-Stokes equation where so-called non-linear term $\rho(\boldsymbol{v}.\nabla)\boldsymbol{v}$ can be neglected [1]. In this section, two cases of which, Hydrostatic pressure and Poiseuille flow, are discussed.

2.3.1 Hydrostatic pressure

In mechanical equilibrium, the fluid is at rest and therefore, the velocity field is zero throughout the channel, $\boldsymbol{v} = 0$ [1]. In this simple case, if the microchannel is assumed along *z*-axis, the Navier-Stokes equation becomes,

$0 = -\nabla p_{hs} - \rho g e_z$. (2-14)

where, "hs" shows hydrostatic.

For an incompressible fluid, the hydrostatic pressure satisfying above equation is as below,

$p_{hs}(z) = p^* - \rho g z$. (2-15)

where p^* is the pressure at $z=0$.

It shows how a liquid column of height ΔH can apply a pressure difference of $\rho g \Delta H$ between its two ends. For example, a vertical microchannel with 10 cm height filled with water, $\rho g \approx 10^4 Pam^{-1}$, exerts pressure difference of $\Delta p = 1kPa$ [1].

2.3.2 Poiseuille flow

Poiseuille flow is a steady-state flow in a long, rigid, fixed-shape cross section channel that is only caused by pressure difference through channel [1]. If the channel length is assumed to be along x-axis, the velocity has only one component along this axis and this component is only a function of y and z, i.e., $\boldsymbol{v} = \boldsymbol{v}_x(y,z)e_x$. Therefore, the non-linear term of $(\boldsymbol{v}.\nabla)\boldsymbol{v} = (\boldsymbol{v}_x\partial_x)\boldsymbol{v}_x(y,z)e_x = 0$ will be zero [1]. Herein, no-slip boundary condition is assumed for channel surface implying zero velocity at walls of microchannel [1]. The new form of Navier-Stoke equation for steady state Poiseuille flow is,

$$\boldsymbol{v}(r) = \boldsymbol{v}_x(y,z)e_x \qquad (2\text{-}16)$$

$$0 = -\nabla p + \eta\nabla^2[\boldsymbol{v}_x(y,z)e_x]. \qquad (2\text{-}17)$$

Based on the above equations, because velocity vector has only $\boldsymbol{x}$-component, it leads $\partial_y p$ and $\partial_z p$ to be zero and therefore the pressure field is only a function of $\boldsymbol{x}$coordinate, $p(r) = p(x)$ [1], equation (2-17) can be rewritten,

$$\eta\left[\partial_y^2 + \partial_z^2\right]\boldsymbol{v}_x(y,z) = \partial_x p(x). \qquad (2\text{-}18)$$

The only possible solution for equation (2-18) is a constant for both sides[1]. Therefore, the pressure field by considering boundary conditions, is found,

$$p(0) = \Delta p + p^* \quad \text{and} \quad p(L) = p^*\,, \qquad (2\text{-}19)$$

$$p(r) = \frac{\Delta p}{L}(L - x) + p^*. \qquad (2\text{-}20)$$

By substituting equation (2-20) into (2-18) and assuming the cross-section $\boldsymbol{C}$with slip boundary conditions at the solid walls $\partial\Omega$ [1], partial differential equation for $\boldsymbol{v_x}(y,z)$ is,

$$\left[\partial_y^2 + \partial_z^2\right]\boldsymbol{v}_x(y,z) = -\frac{\Delta p}{\eta L}, \quad \text{for } (y,z) \in C \qquad (2\text{-}21)$$

$$\boldsymbol{v}_x(y,z) = 0, \text{ for } (y,z) \in \partial\Omega. \qquad (2\text{-}22)$$

Bruss [1] has shown analytical solution for velocity in some microchannel with specific cross section, particularly, circular with radius a and rectangular $-\frac{1}{2}w < y < \frac{1}{2}w$,

$$\boldsymbol{v}_x(y,z) = \frac{\Delta p}{4\eta L}(a^2 - y^2 - z^2), \text{ circular tube} \qquad \text{(2-23a)}$$

$$\boldsymbol{v}_x(y,z) = \frac{4h^2\Delta p}{\pi^3 \eta L}\sum_{n,odd}^{\infty}\frac{1}{n^3}\left[1 - \frac{\cosh\left(n\pi\frac{y}{h}\right)}{\cosh\left(n\pi\frac{w}{2h}\right)}\right], \text{ rectangular section } h < w \text{ .} \qquad \text{(2-23b)}$$

Once particles are released in a microchannel, they follow Poiseuille-flow velocity field $\boldsymbol{v}_x(y,z)$. Figure 2-1 shows COMSOL simulation of $10\,\mu m$ MPs velocity captured 1 second and 6 seconds after being released in a microchannel with dimensions of $W \times H = 13\,mm \times 0.11\,mm$. This Figure shows how 10 µm MPs follow the profile velocity of rectangular microchannel with mean inflow velocity of 0.6 mm/s. As shown in this Figure, the particles at the middle of microchannel height enjoying maximum velocity while those closer to the walls, have the minimum velocity.

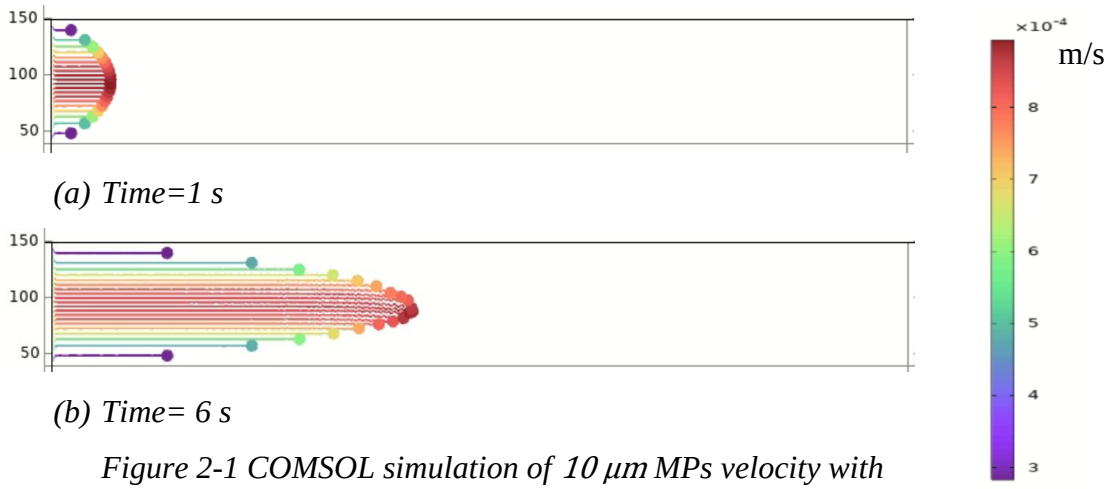

(a) Time=1 s

(b) Time= 6 s

Figure 2-1 COMSOL simulation of $10\,\mu m$ MPs velocity with density of $950\ kg/m^3$ at two times 1s and 6s. Color column shows the velocity (m/s)

3 Perturbation Theory and acoustic resonance

Ultrasound acoustics in frequencies $f > 1.5\,MHz$ that result in wavelength $\lambda_{wa} \leq 1mm$, for water, are suited well for microchannel and cavities which are in dimension of submillimetre [8]. It leads to standing pressure waves or resonance modes that are not only stable and reproducible; they can also be controlled by the geometry of microchannel. At resonance, one can transfer maximum power from, for example, piezoelectric transducer to particles suspended in microchannel through acoustic radiation force or acoustic streaming [8]. Piezoelectric transducers can generate waves in the form of bulk or surface acoustic waves.

Understanding perturbation theory for deriving acoustic radiation force and streaming is of importance. In this chapter, after introducing first order and second order perturbation theory in microfluidics, acoustic resonance in microchannel will be discussed. To do so, this chapter follows process and equations used in reference [8] by Bruss. The basic derivation equations are kinematic continuity for ρ and the dynamic Navier-Stokes equation for the velocity $\boldsymbol{v}$ [8],

$$p = p(\rho), \tag{3-1a}$$

$$\partial_t \rho = -\nabla.(\rho \boldsymbol{v}), \tag{3-1b}$$

$$\rho \partial_t \boldsymbol{v} = -\nabla p - \rho(\boldsymbol{v}.\nabla)\boldsymbol{v} + \eta\nabla^2\boldsymbol{v} + \beta\eta\nabla(\nabla.\boldsymbol{v}). \tag{3-1c}$$

In this chapter, all external forces like gravity are neglected and, for simplification, the temperature is assumed constant (isothermal case).

3.1 First-order perturbation theory

Before perturbation, liquid is assumed at rest where it has constant density ρ_0 and pressure p_0, a tiny perturbation (subscript 1) by an acoustic wave causes changes in the fields of density ρ, pressure p and velocity $\boldsymbol{v}$ [8],

$$\rho = \rho_0 + \rho_1, p = p_0 + {c_a}^2\rho_1, \text{ and } \boldsymbol{v} = \boldsymbol{v}_1. \tag{3-2}$$

In the expansion of pressure, isentropic state is considered [8],

$$p(\rho) = p_0 + (\partial p/\partial \rho)_s \rho_1. \quad (3\text{-}3)$$

Bruss in reference [8] has shown that the derivative in equation (3-3) enjoys the dimension of a velocity squared and is equal the speed of sound in liquid, ${c_a}^2$.

By inserting equation (3-2) into equation (3-1) and doing some mathematical manipulation [8], resulting expression is,

$${\partial_t}^2 \rho_1 = {c_a}^2 \left[1 + \frac{(1+\beta)\eta}{\rho_0 {c_a}^2} \partial_t\right] \nabla^2 \rho_1. \quad (3\text{-}4)$$

By assuming harmonic time dependence of all fields [8],

$$\rho_1(r,t) = \rho_1(r) e^{-i\omega t}, \quad (3\text{-}5a)$$
$$p_1(r,t) = {c_a}^2 \rho_1(r) e^{-i\omega t}, \quad (3\text{-}5b)$$
$$\boldsymbol{v}_1(r,t) = \boldsymbol{v}_1(r) e^{-i\omega t}, \quad (3\text{-}5c)$$

Where in $\omega = 2\pi f$, f is the frequency of acoustic field.

By considering equations (3-3) and (3-4), the equation for the pressure (Helmholtz equation) is found [8],

$$\nabla^2 p_1 = -k^2 p_1, \quad (3\text{-}6a)$$
$$k = (1 + i\gamma) k_0 = (1 + i\gamma) \frac{\omega}{c_a}, \quad (3\text{-}6b)$$
$$\gamma = \frac{(1+\beta)\eta\omega}{2\rho_0 {c_a}^2} \approx 10^{-6}. \quad (3\text{-}6c)$$

Where k_0 and k are the wavenumber and complex-valued wavenumber and γ is the viscous damping factor that is almost 10^{-6} for water at $f = 1\ MHz$.

By neglecting the viscosity in the bulk part of acoustic wave, equation (3-3) can be rewritten in a standard wave equation [8],

$$\nabla^2 p_1 = \frac{1}{{c_a}^2}\partial_t{}^2 p_1, \quad \text{for } \eta = 0 \qquad (3\text{-}7)$$

Bruss in reference [8] has shown that in an inviscid microfluid, velocity and density can be found from pressure,

$$v_1 = -i\frac{1}{\rho_0\omega}\nabla p_1 = \nabla \emptyset_1, \quad \text{for } \eta = 0 \qquad (3\text{-}8a)$$

$$\emptyset_1 = \frac{-i}{\rho_0\omega} p_1, \quad \text{for } \eta = 0 \qquad (3\text{-}8b)$$

where $\emptyset_1$ is defined as potential of velocity [8].

3.2 Second-order perturbation theory

For having more accurate solution for the nonlinear dynamic Navier-Stokes equation, first order expansion of pressure, density and velocity fields in equation (3-2) can be continued to second order one as below [8],

$$p = p_0 + p_1 + p_2, \qquad (3\text{-}9a)$$

$$\rho = \rho_0 + \rho_1 + \rho_2, \qquad (3\text{-}9b)$$

$$\boldsymbol{v} = 0 + \boldsymbol{v}_1 + \boldsymbol{v}_2, \qquad (3\text{-}9c)$$

Where all zero and first order terms are given or calculated.

One can express second-order equations of state, continuity and Navier-Stokes as below [8],

$$p_2 = {c_a}^2\rho_2 + \frac{1}{2}(\partial_\rho {c_a}^2)_0 {\rho_1}^2, \qquad (3\text{-}10a)$$

$$\partial_t \rho_2 = -\rho_0 \nabla.\boldsymbol{v}_2 - \nabla.(\rho_1 \boldsymbol{v}_1), \qquad (3\text{-}10b)$$

$$\rho_0 \partial_t \boldsymbol{v}_2 = -\nabla p_2 + \eta\nabla^2 \boldsymbol{v}_2 + \beta\eta\nabla(\nabla.\boldsymbol{v}_2) - \rho_1 \partial_t \boldsymbol{v}_1 - \rho_0(\boldsymbol{v}_1.\nabla)\boldsymbol{v}_1. \qquad (3\text{-}10c)$$

The time average of an oscillating quantity $X(t)$ over its period τ is defined as,

$$\langle X \rangle \equiv \frac{1}{\tau}\int_0^\tau dt\, X(t). \qquad (3\text{-}11)$$

Since the time-average of $\langle \cos(\omega t) \rangle$ is equal zero, time-average effect of first-order fields will be zero [8], see equations (3-5). Therefore, only second-order terms do participate in time average quantities such as radiation force, will be discussed in chapter 4. Time average of second order equations of continuity and Navier-Stokes, equation (3-10), becomes [8],

$$\rho_0 \nabla . \langle \boldsymbol{v}_2 \rangle = -\nabla . \langle \rho_1 \boldsymbol{v}_1 \rangle, \quad (3\text{-}12a)$$

$$\eta \nabla^2 \langle \boldsymbol{v}_2 \rangle + \beta \eta \nabla (\nabla . \langle \boldsymbol{v}_2 \rangle) - \nabla \langle p_2 \rangle = \langle \rho_1 \partial_t \boldsymbol{v}_1 \rangle + \rho_0 \langle (\boldsymbol{v}_1 . \nabla) \boldsymbol{v}_1 \rangle. \quad (3\text{-}12b)$$

3.3 Boundary conditions and acoustic resonance

Acoustic resonance modes are widely used to handle bioparticles or other particles in microfluidics [8]. In these modes, maximum energy can be transferred from piezoelectric actuator to microchannel containing fluid with suspended particles.

3.3.1 Boundary conditions

Boundary conditions are required to find exact solution of eigenmodes $p_n = p_n(r) e^{-i\omega_n}$ that are the solutions of Helmholtz equation (3-6). There are three main boundary conditions discussed in reference [8],

$$p_1 = 0, \quad \text{soft-wall boundary conditions} \quad (3\text{-}13a)$$

$$n . \nabla p_1 = 0, \quad \text{hard-wall boundary conditions} \quad (3\text{-}13b)$$

$$n . \nabla p_1 = i \frac{\omega \rho_0}{\rho_m c_m} p_1, \quad \text{lossy-wall boundary conditions} \quad (3\text{-}13c)$$

Lossy-wall condition is associated with partial acoustic loss between liquid and surrounding medium [8]. Liquid/air interface or thin glass wall and silicon/glass chips surrounded microchannel, $(\rho_{si} c_{si})/ (\rho_{wa} c_{wa})$=13.2, are the examples of soft-wall and hard-wall boundary conditions respectively [8].

3.3.2 Resonance in water-filled rectangular channel

Resonance happens at special frequencies ω_j, $j=1,2,3,\ldots$ that depend on microchannel geometries and material parameters [21]. Resonance frequencies can be found analytically for some acoustic microchannel, one of which is a rectangular channel of length l, width w, and height h filled with water and surrounded by infinitely soft or hard acoustic material [8]. It can be seen that following eigenmodes can easily satisfy Helmholtz equation for such rectangular microchannel[8],

$$p_1(x,y,z) = p_a \sin(k_x x)\sin(k_y y)\sin(k_z z), \quad \text{(3-14a)}$$

with $k_j = n_j \frac{\pi}{L_j}$, where $(L_x, L_y, L_z) = (l, w, h)$ and $n_j = 0,1,2,\ldots$ soft wall,

$$p_1(x,y,z) = p_a \cos(k_x x)\cos(k_y y)\cos(k_z z), \quad \text{(3-14b)}$$

with $k_j = n_j \frac{\pi}{L_j}$, where $(L_x, L_y, L_z) = (l, w, h)$ and $n_j = 0,1,2,\ldots$ hard wall,

where p_a is pressure amplitude and opposite corners of rectangular microchannel are placed at $(0,0,0)$ and (l, w, h) the coordinate system.

Figure 3-1 shows two simulated pressure field p_1 at resonant modes $(n_x, n_y, n_z) = (0,1,0)$ with $f_{0,1,0} = 1.48\ MHz$ and $(n_x, n_y, n_z) = (3,1,0)$ with $f_{3,1,0} = 1.55\ MHz$ of a water-filled rectangular microchannel with length $l = 5mm$, width $w = 0.5mm$, and height $h = 0.2mm$ along x,y, and z axis respectively [21].

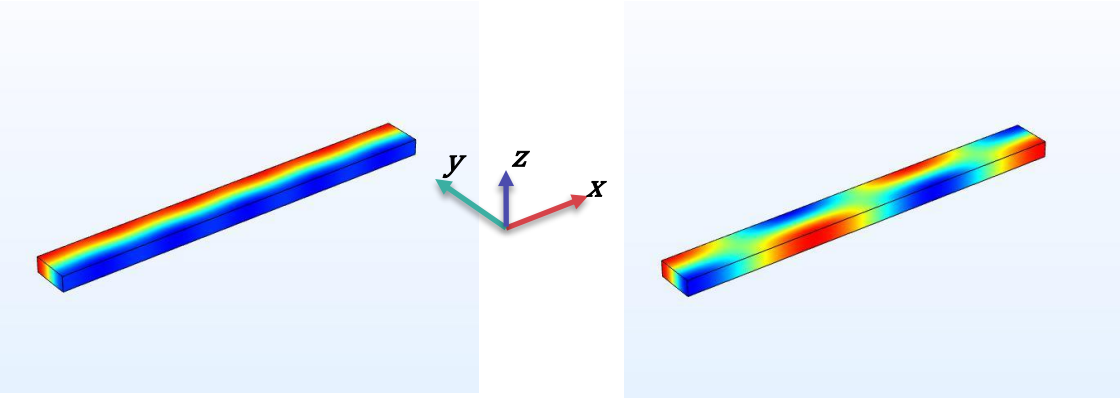

(a) *(b)*

Figure 3-1 COMSOL simulation of pressure field p_1 *at resonant modes* $(n_x, n_y, n_z) = (0,1,0)$ *with* $f_{0,1,0} = 1.48\ MHz$ *and* $(n_x, n_y, n_z) = (3,1,0)$ *with* $f_{3,1,0} = 1.55\ MHz$ *of a water-filled rectangular microchannel with length* $l = 5mm$*, width* $w = 0.5mm$*, and height* $h = 0.2mm$ *along x,y, and z axis. Colors show the sign of pressure as red: positive, green: zero, and blue: negative.*

4 Acoustic radiation force and acoustic streaming

Acoustic radiation force (ARF) and acoustic streaming are two important phenomena in acoustofluidics that are extracted analytically from perturbation method [22], [23]. With recent advancement in deployment ultrasound resonators in lab-on-chip systems in which bioparticles are manipulated through acoustic radiation force and streaming [22], it is important to study these effects and investigate acoustofluidics parameters that play role in manipulating sub-micron and microparticles.

This chapter starts with presenting formulas used for computing acoustic radiation force, which is experienced by a small particle, followed by introducing acoustic streaming as a steady flow field in the fluid.

4.1 The acoustic radiation force on small particles

When the pressure in a fluid changes over time, the suspended particles in the fluid experience a time-averaged force resulted from scattering of the acoustic waves on the particles [22]. The expression for acoustic radiation force is extracted from a perturbation expansion of the acoustic fields, see equations 3-9, and the first order continuity and Navier-Stokes equations [12]:

$$\partial_t \rho_1 = -\rho_0 \nabla . \boldsymbol{v}_1, \quad (4\text{-}1a)$$

$$\rho_0 \partial_t \boldsymbol{v}_1 = -c_0^2 \nabla p_1 + \eta \nabla^2 \boldsymbol{v}_1 + \beta \eta \nabla (\nabla . \boldsymbol{v}_1). \quad (4\text{-}1b)$$

where η is the dynamic viscosity of the fluid and β the viscosity ratio typically of the order of unity [12].

Bruus in the part 7 of the thematic tutorial series “Acoustofluidics — exploiting ultrasonic standing waves, forces and acoustic streaming in microfluidic systems for cell and particle manipulation” has shown the derivation process of acoustic radiation force for “ a compressible, spherical, micro-meter-sized particle of a radius *a* suspended in an inviscid fluid in an ultrasound field of wavelength λ” [22]. The expression for ARF is valid for particles much smaller than wavelength, i.e. $a \ll \lambda$, with density ρ_p and compressibility

κ_p [22]. This approach is a traditional way of driving ARF through neglecting viscosity, however, as Settnes and Bruus show [12], it is almost valid for cases in which particles are much larger than the thickness of the acoustic boundary layer or viscous penetration length shown by δ:

$$\delta = \sqrt{\frac{2\vartheta}{\omega}} \qquad (4\text{-}2)$$

where, ϑ and ω are kinematic viscosity and angular frequency.

For example, this value equals to 0.6 μm for 1 MHz ultrasound frequency in water at room temperature [12]. Therefore, for particles with radius larger than 3 μm, one can use ARF formula for inviscid fluid. However, with advancement in microelectromechanical technology, there is a need for better accuracy as well as manipulating small particles. As a result, it is recommended to consider the effect of viscosity in fluid bulk on acoustophoresis [12].

Herein, only resulting expression for the radiation force experienced by a small particle ($\delta, a \ll \lambda$) has been shown, however, readers can follow theory and procedures for driving such formula through reading references [14] and [16].

$$\boldsymbol{F}^{rad} = -\pi a^3 \left[\frac{2\kappa_0}{3} Re[f_1^* p_{in}^* \nabla p_{in}] - \rho_0 Re[f_2^* \boldsymbol{v}_{in}^* . \nabla \boldsymbol{v}_{in}]\right], \qquad (4\text{-}3)$$

where κ_0 is the compressibility of fluid, $\kappa_0 = \frac{1}{\rho_0 c_0^2}$.

f_1 and f_2 are monopole and dipole scattering coefficients and can be found by following equations[12]:

$$f_1(\tilde{\kappa}) = 1 - \tilde{\kappa}, \quad \text{with} \quad \tilde{\kappa} = \frac{\kappa_p}{\kappa_0} \qquad (4\text{-}4)$$

$$f_2(\tilde{\rho}, \tilde{\delta}) = \frac{2[1-\gamma(\tilde{\delta})](\tilde{\rho}-1)}{2\tilde{\rho}+1-3\gamma(\tilde{\delta})}. \quad \text{with } \tilde{\rho} = \frac{\rho_p}{\rho_0} \text{ and } \gamma(\tilde{\delta}) = -\frac{3}{2}\left[1 + i\left(1 + \tilde{\delta}\right)\right]\tilde{\delta}. \qquad (4\text{-}5)$$

where $\tilde{\delta}$ is an important dimensionless parameter is given by $\tilde{\delta} = \frac{\delta}{a}$.

Based on the above equations, $f_1(\tilde{\kappa})$ is a real-valued that is only a function of the compressibility ratio. However, $f_2(\tilde{\rho}, \tilde{\delta})$ that is related to viscosity, defines the

translational movement of the particle, an important parameter in ARF arising from travelling acoustic waves [12].

4.1.1 Final expressions for the radiation force

To sum up, based on reference [12], one can use following equations, some questions have been overwritten, for calculating ARF arising from standing acoustic wave and travelling planar wave on a suspended small particle ($a \ll \lambda$) in a fluid with viscosity η, density ρ_0, and compressibility κ_0.

For a standing acoustic wave:

$$\boldsymbol{F}^{rad} = \frac{4\pi}{3} a^3 \left[f_1 \frac{1}{2} \kappa_0 \langle p_{in}^2 \rangle - f_2^r \frac{3}{4} \rho_0 \langle \boldsymbol{v}_{in}^2 \rangle \right], \quad (4\text{-}6a)$$

$$f_1(\tilde{\kappa}) = 1 - \tilde{\kappa}, \quad \text{with} \quad \tilde{\kappa} = \frac{\kappa_p}{\kappa_0} \quad (4\text{-}6b)$$

$$f_2^r(\tilde{\rho}, \tilde{\delta}) = Re\left[f_2(\tilde{\rho}, \tilde{\delta})\right] = Re\left[\frac{2[1-\gamma(\tilde{\delta})](\tilde{\rho}-1)}{2\tilde{\rho}+1-3\gamma(\tilde{\delta})}\right], \quad \text{with } \tilde{\rho} = \frac{\rho_p}{\rho_0} \quad (4\text{-}6c)$$

$$\gamma(\tilde{\delta}) = -\frac{3}{2} Re\left[1 + i(1+\tilde{\delta})\right]\tilde{\delta}, \text{ with } \tilde{\delta} = \frac{\delta}{a} \quad (4\text{-}6d)$$

For a travelling planar wave:

$$\boldsymbol{F}^{rad} = f_2^i(\tilde{\rho}, \tilde{\delta}) \pi a^3 \rho_0 \langle \boldsymbol{v}_{in}^2 \rangle \boldsymbol{k}, \quad (4\text{-}7a)$$

$$f_2^i(\tilde{\rho}, \tilde{\delta}) = Im\left[f_2(\tilde{\rho}, \tilde{\delta})\right] = \frac{6(1-\tilde{\rho})^2(1+\tilde{\delta})\tilde{\delta}}{(1+2\tilde{\rho})^2+9(1+2\tilde{\rho})\tilde{\delta}+\frac{81}{2}(\tilde{\delta}^2+\tilde{\delta}^3+\frac{1}{2}\tilde{\delta}^4)}, \quad (4\text{-}7b)$$

Where $\boldsymbol{k}$ is wave number which is parallel to $v_{in}[12]$.

4.1.2 Acoustic radiation force factor

The acoustic radiation force factor $\boldsymbol{F}_F$ is defined as the ratio of F^{rad} [N] over unit acoustic energy density [J/m^3] on unit cross sectional area of the particle [m^2] [6]. Figure 4-1 shows the diagram of acoustic radiation force factor $\boldsymbol{F}_F$ based on the frequency for a range of polystyrene (PS) particle diameter [6]. In this diagram, κ is a dimensionless factor, defined as below:

$$\kappa = \frac{2\pi}{\lambda} a. \quad (4\text{-}8)$$

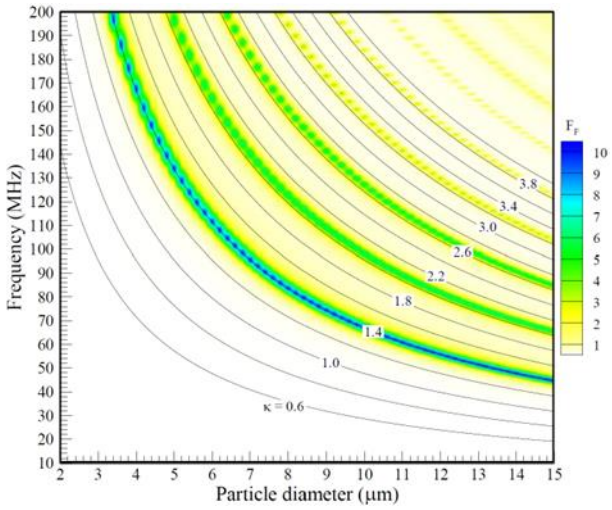

Figure 4-1 contour plot of acoustic radiation force factor F_F depicted for a wide range of frequency and particle diameter based on κ factor [6].

Several studies have shown that for having an effective translation of particles, κ should be greater than one, for example for PS particles $\kappa \geq 1.3$ [4]. Moreover, based on this plot, one can choose a working frequency based on which only one group of particles with a specific diameter can be isolated from other groups of particles having different sizes. For example, Destgeer, et al., have employed this technique to separate 3, 4.2 and 5 μm particles from each other in a continuous flow through using only one slanted interdigitated transducer (SIDT) actuating with 165 MHz frequency [6].

4.2 Acoustic streaming

Sadhal in the part 13 of the thematic tutorial series "Acoustofluidics — exploiting ultrasonic standing waves, forces and acoustic streaming in microfluidic systems for cell and particle manipulation" has analysed acoustic streaming through perturbation method [23]. Here, only this phenomenon is described without providing any mathematical analysis, however, for those who are interested, they can read references [23]–[25] for being more familiar with governing equations and applications of acoustic streaming.

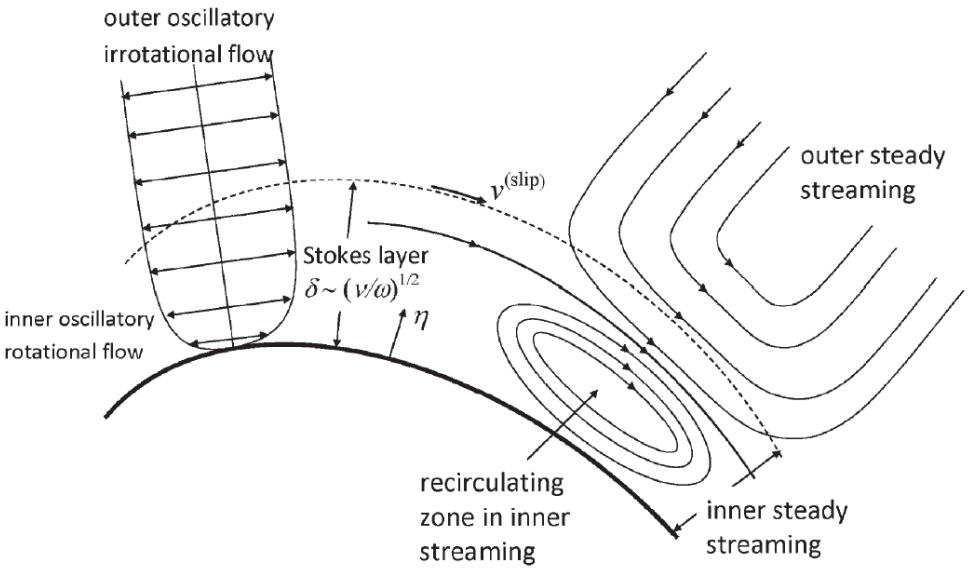

Figure 4-2 *Schematic of different flow in Stokes layer δ and bulk of fluid* [23]

Streaming can be classified into boundary-driven and attenuation driven types [9]. For boundary-driven streaming, as an example, when a body with dimension a oscillates with velocity $U_0 \cos(\omega t)$ in which U_0 and ω are amplitude and angular frequency of oscillation respectively, with the condition $\varepsilon = U_0/\omega a \ll 1$, the acoustic velocity field not only has leading order solution such as $\cos(\omega t)$, but it has also higher order terms, for example, $cos^2(\omega t) = \frac{1}{2}(1 + \cos(2\omega t))$, where the term $\frac{1}{2}$ is a steady state component associated with acoustic streaming. This stream field causes a recirculating zone (vorticity) in Stokes layer with thickness $\delta = (\vartheta/\omega)^{\frac{1}{2}}$ above the solid surface that induces a steady streaming field in the bulk of fluid, see Figure 4-2 [23].

Acoustic streaming can also happen when the attenuation length in fluid is comparable with microchannel dimensions [4]. In this case, amplitudes of pressure and velocity decrease gradually through propagation direction of wave resulting a force parallel to the planar wave [23]. For example, Figure 4-3 shows the result of a simulation where MPs with $2\mu m$ diameter are moved through water-filled microchannel by streamline and start to rotate when they are trapped in a vorticity formed in the bulk of fluid. Here, the actuation frequency of surface acoustic wave (SAW) resonator is 358.5 MHz resulting acoustic wave attenuation length of $3 \times 10^6 \lambda_{TSAW}^2 = 51.3\mu m$ in the fluid. The microchannel hight is $H = 110\mu m$.

(a)

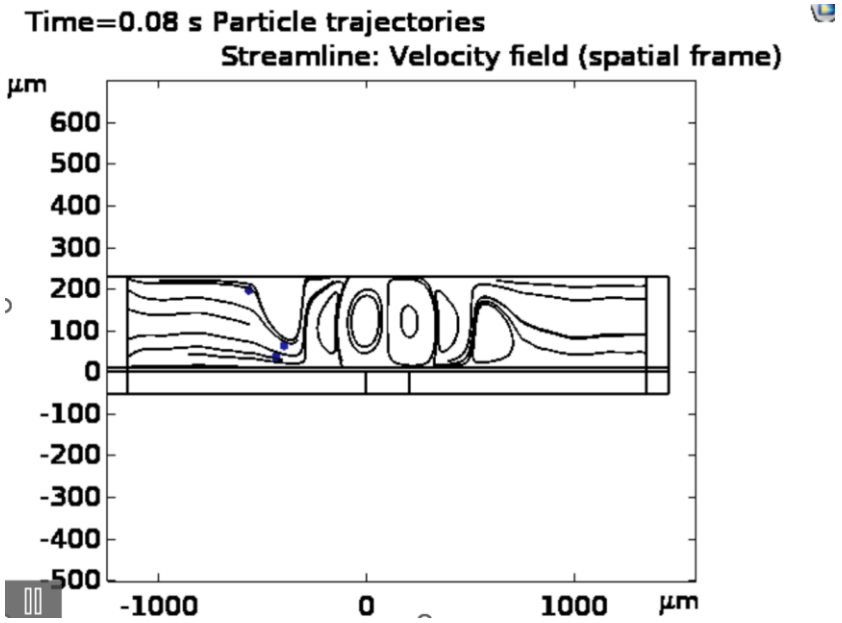

(b)

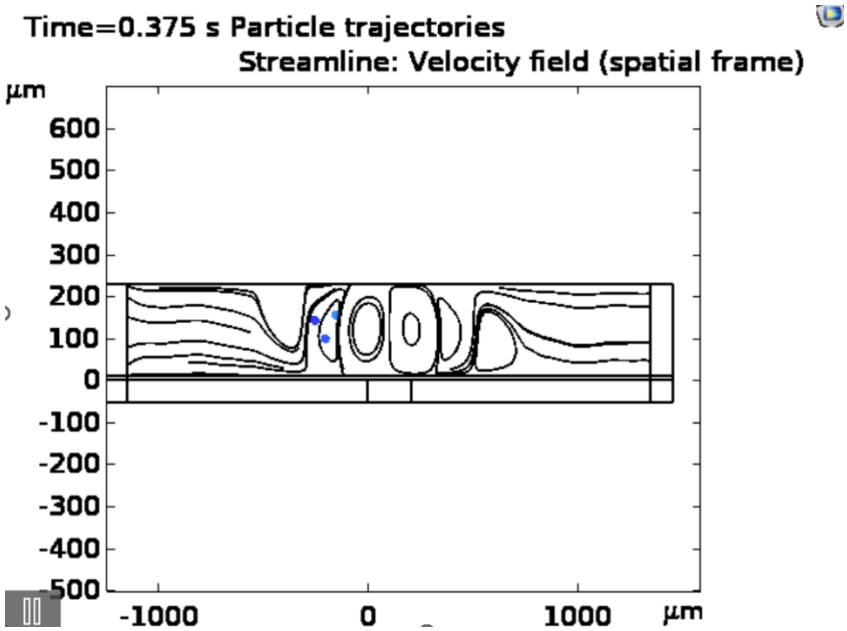

Figure 4-3 Streamline with vortices in a microchannel and blue colored 2µm MPs at (a) following streamline up until (b) trapped in a vorticity at bulk of fluid.

In the simulation, Figure 4-3, that is carried out in COMSOL, the main driving force defining particles trajectories is streaming-induced Stokes drag force,

$$\boldsymbol{F}^{drag} = 6\pi\eta a\left(\boldsymbol{v}_2 - \boldsymbol{v}_p\right) \qquad (4\text{-}9)$$

where v_2 and v_p are streaming velocity and particle velocity respectively. Fluid viscosity and particle radius is shown by η and a.

5 Model description and simulation results in COMSOL

This chapter deals with description of modelling process of proposed acoustofluidics platform, followed by simulation results in COMSOL. Steps of modelling has been described based on the order of nodes and interfaces used in COMSOL. The simulation of model has been inspired by the tutorial model of "Acoustic Streaming in a Microchannel Cross Section" available in the application libraries of COMSOL 6.1 [26].

Figure 5-1 shows the flow chart of implementing numerical model for simulating particles trajectories in acoustofluidics utilizing travelling surface acoustic waves. As shown in this flow chart, the modelling starts with simulating a unit cell of SAW resonator to find the resonant frequency of resonator. Then by making an array of the unit cell, the completed SAW resonator has been modelled following adding layers of PDMS and water. Afterwards, the resonant frequency of SAW resonator with added load of PDMS and water was extracted through sweeping frequency in frequency domain study. Traveling acoustic fields of pressure and velocity were simulated at resonant frequency to be used in calculating acoustic radiation force. Acoustic streaming is also simulated through stationary study of laminar flow to extract streaming-induced Stokes drag force. Finally, these forces are used to simulate particles trajectories.

5.1 SAW resonator

Surface acoustic wave (SAW) resonator causes a wave propagation which is mostly confined along the surface of a piezoelectric material. This transducer which is also called interdigitated transducer (IDT) is usually comprised of a set of electrodes that are placed periodically on the piezoelectric substrate, see Figure 5-2(a) [27]. By applying alternating voltage to the electrodes, piezoelectric substrate converts electrical energy to mechanical one resulting the surface acoustic waves.

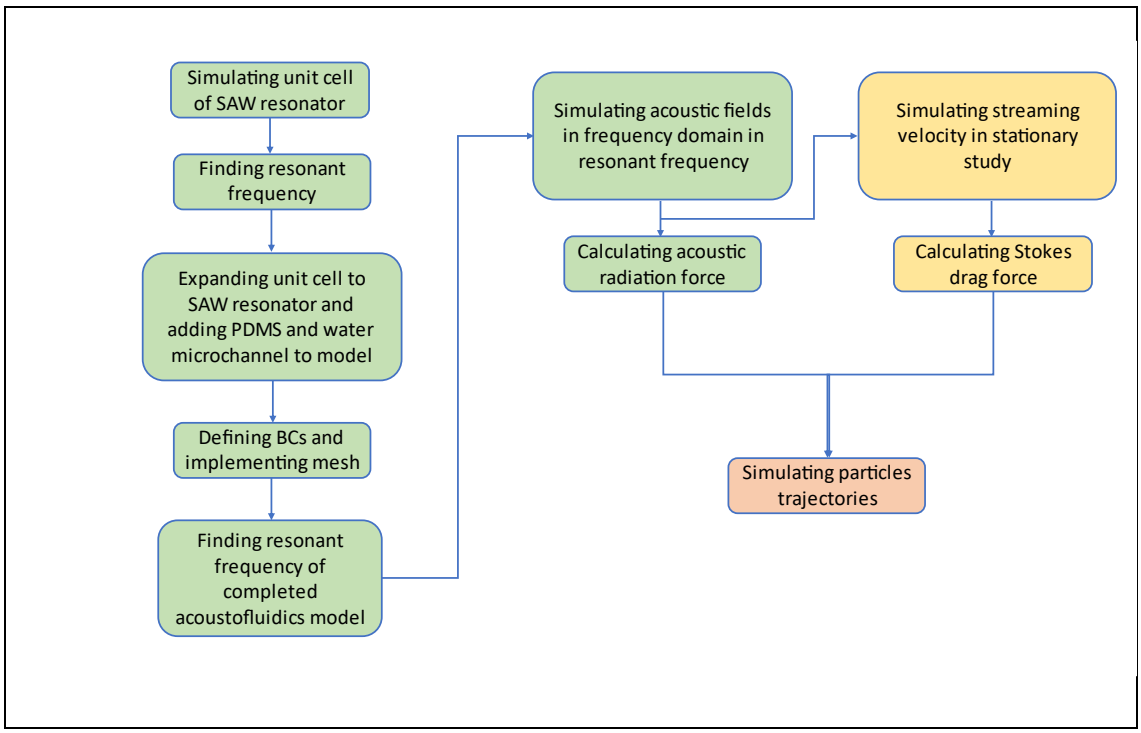

Figure 5-1 flow chart of numerical model for simulating particles trajectories in acoustofluidics devices utilizing travelling surface acoustic waves.

Figure 5-2(a) and (b) shows a 3D schematic view of a SAW resonator with highlighting a unit cell of a this resonator, captured from [27], and a unit cell of SAW resonator which is simulated in COMSOL to obtain the resonant frequency and the corresponding mode shape. The length of this unit cell is equal to the resonator wavelength (λ_{TSAW}) and is set 53 μm. This wavelength corresponds to the frequency of 72.4 MHz in which, based on Figure 4-1 in chapter 4, 10 μm Polystyrene particles experience an effective translational motion. Since acoustic energy exponentially decays in the bulk of piezoelectric after a few wavelengths, the height of Lithium Niobate 128 Y-X cut is considered 5 times of wavelength to decrease the computational cost of simulation [27]. The Aluminum electrode coverage ratio is 0.5. Thickness of Aluminum electrodes and insulator is 0.2 µm and 0.4 µm respectively. In terms of boundary conditions, periodic boundary with continuity type is applied at the left and right sides of model as well as the substrate is fixed constraint at the bottom. Figures 5-2(c) and (d) show mode shape and the electrical admittance (S) of the unit cell. Based on these diagrams, the resonance frequency of SAW resonator is 73.5 MHz.

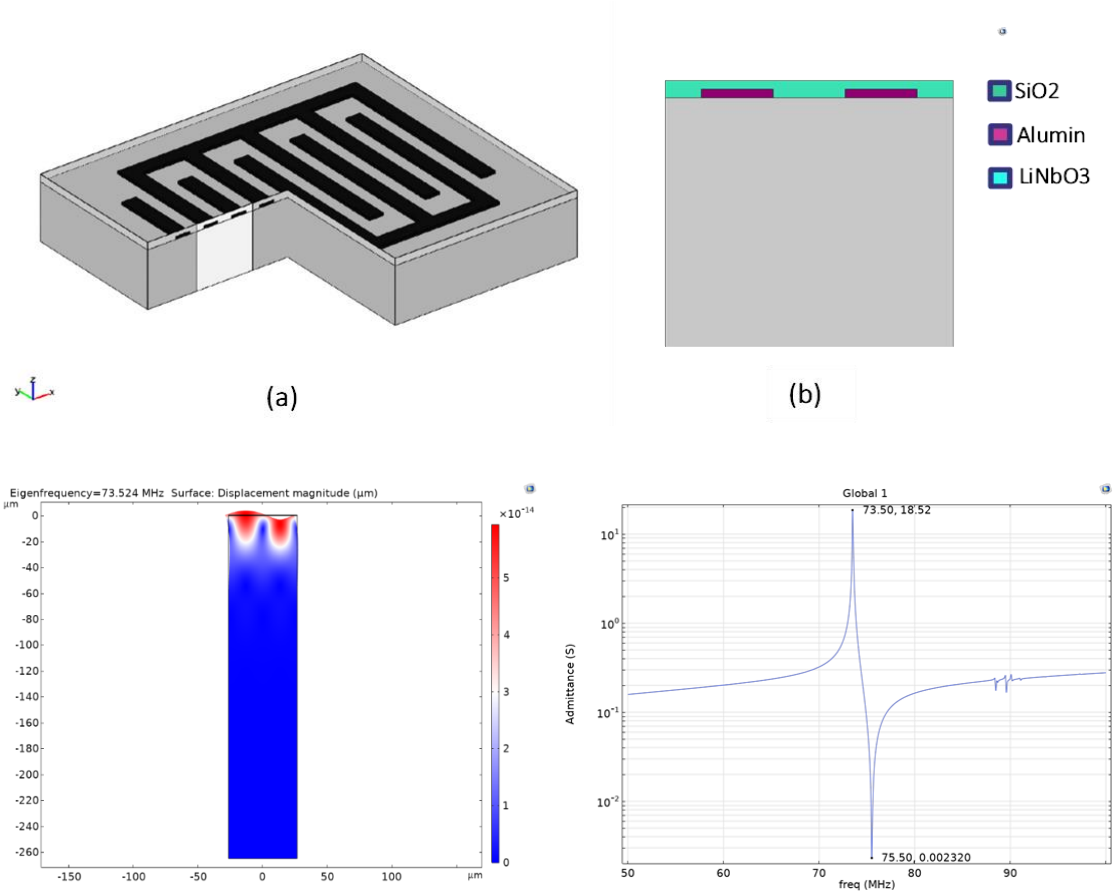

Figure 5-2(a) 3D schematic view of SAW resonator captured from [27], (b) 2-D model of the unit cell of SAW resonator simulated in COMSOL, (c) the mode shape in frequency of 73.524 MHz with deformation scale factor of 0.6E14 and (d) electrical admittance showing resonant at 73.5 MHz

The completed model of SAW resonator consists of 20 pairs electrodes by making array of the first simulated unit cell. Perfectly matched layers (PMLs) are used at both sides of substrate to attenuate acoustic energy. Bottom of piezoelectric substrate is fixed constraint. Figure 5-3 shows the electrical admittance of the SAW resonator utilized in the main model, see Figure 5-4. Based on this diagram, the resonance frequency of SAW resonator, which is used in frequency domain study to simulate acoustic fields, is 72.4 MHz.

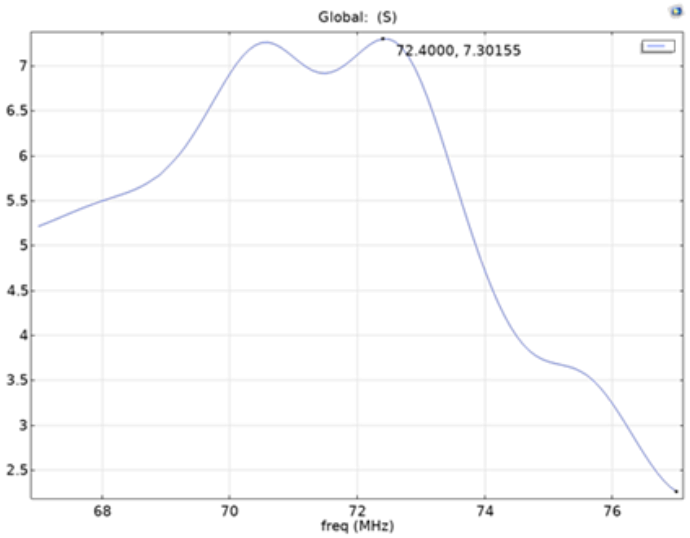

Figure 5-3 Diagram of electrical admittance of SAW resonator utilized in the acoustofluidics model which shows resonant frequency at 72.4 MHz

5.2 Model description in COMSOL

As it is shown in Figure 5-4, the proposed 2D acoustofluidics model is designed and simulated in COMSOL Multiphysics version 6.1 finite element method software[28]. It comprises 20 pairs uniformly placed electrodes (IDT) with period length of 53 μm on a Lithium Niobate piezoelectric, 128 Y-X cut, substrate. On top of electrodes, there are layers of SiO2, PDMS and water-filled rectangular microchannel respectively. Table 5-1 shows dimensions of different geometries of the model.

5.2.1 Process steps of modelling in COMSOL

For modelling the proposed acoustofluidics model, physics of Solid Mechanics (Solid), *Electrostatics (es)*, *Pressure Acoustics Frequency Domain (acpr)*, *Laminar Flow (spf),* and *Particle Tracing for Fluid Flow (fpt)* as well as studies of *Frequency Domain, Stationary*, and *Time Dependent* have been deployed. Temperature (T=20[degC]) and absolute pressure ($P_A = 1[atm]$) are constant for model input.

Table 5-1 *Dimension of layers geometries of the model shown in figure 5-4*

2D Block	Dimensions (μm^2)
Lithium Niobate (LiNbO3)	13780×265
Aluminium electrodes (Al)	13.25×0.2
Silicon Oxide (SiO2)	13780×0.4
Polydimethylsiloxane (PDMS)	13780×38
Water-filled microchannel	13780×110

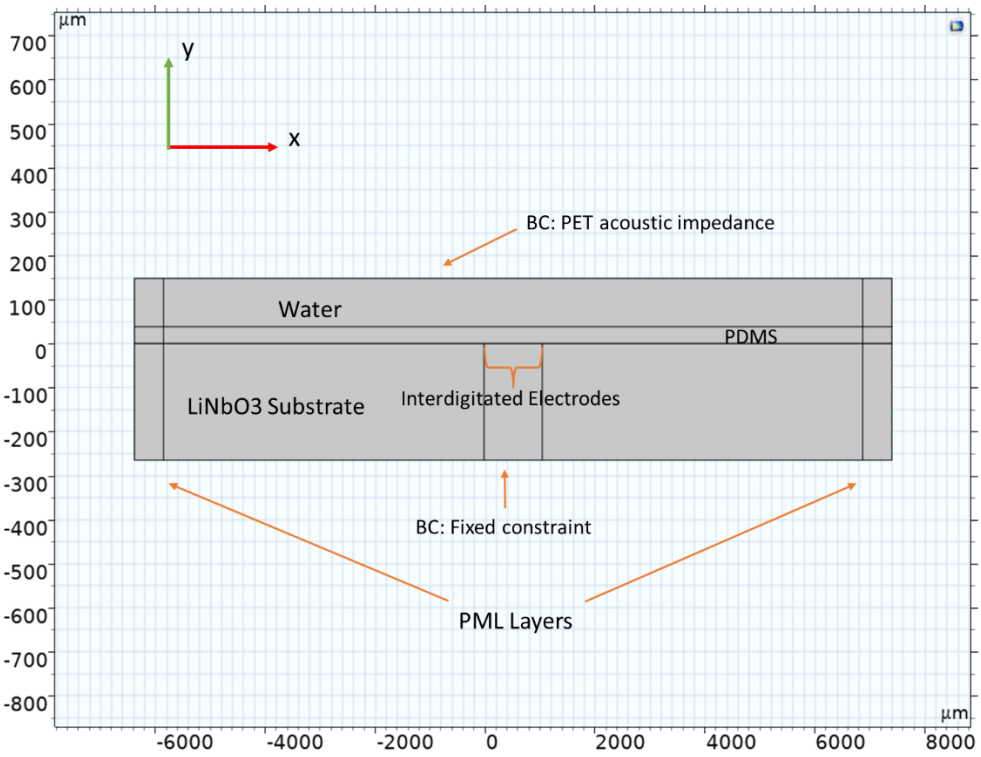

Figure 5-4 2-D 2D acoustofluidics model designed and simulated in COMSOL showing different geometries and boundary conditions

5.2.1.1 Geometry

Creating the geometry of model started with drawing a unit cell of SAW resonator, see Figure 5-2, followed by making linear array with size 20, number of electrode pairs, and periodicity as much as one wavelength, i.e. 53 µm. The width of electrodes is equal to distance between them and is equal to one quarter of wavelength. Between electrodes

and on the top of them, there is a layer of silicon oxide insulator with total height of 0.4 µm. The insulator can protect electrodes from mechanical damages, for example.

Since the wave propagation decays exponentially in depth of substrate regarding the wavelength, the height of LiNbO3, 128 Y-X cut, substrate is assumed 5 times of wavelength to save computational cost of simulation. The substrate and insulator on top of it have been extended as much as 6360 µm from each side of the active area of the transducer. Then a layer of PDMS with thickness of 38 µm was placed on top of insulator. Thickness of PDMS layer should be less than two times of wavelength (λ_{TSAW}) to maintain acousto-thermal effect lower than ARF effect [5]. Finally, water-filled microchannel with height of 110 μm was added to the model. For calculating flow rate, the width of microchannel, which is not visible in the 2-D model, has been assumed 500 µm.

As it is shown in Figure 5-4, perfectly matched layer (PML) with width of ten times of wavelength is placed at both ends of model to attenuate the wave energy. Modelling the PMLs is based on the COMSOL tutorial [29]. PML scaling factor and curvature parameters are 1 and 3 respectively. Typical wavelength of PML is equal to $\lambda_{TSAW} = 53\mu m$.

5.2.1.2 Materials

Materials have been chosen from the material library of COMSOL [30]. The materials used are Lithium Niobate, water(liquid), PDMS – Polydimethylsiloxane, SiO2 - Silicon oxide, and Al – Aluminum.

Since the proposed sensor is supposed to measure the amounts of microplastics (MPs) in sea water and oceans, the physical properties of such environment should be considered for material water used in the model. In terms of density, density of water related to the temperature, salinity and pressure and it is usually in range of 1021 $\frac{kg}{m^3}$ at the surface to 1070 $\frac{kg}{m^3}$ at 10 000 meter depth in ocean [31]. For example, based on a study on ecosystems of Barents Sea, a sea located in north of Norway, the density of this seawater is in the range 1026-1038 $\frac{kg}{m^3}$ [31]. Another important physical parameter of water is the speed of sound. Sound velocity in different seawater has an average of 1500 $\frac{m}{s}$ [32].

Given this information, the density and sound velocity of water used in the COMSOL model have been changed to 1030 $\frac{kg}{m^3}$ and 1500 $\frac{m}{s}$ respectively. Other physical parameters provided by COMSOL like viscosity has not been changed.

5.2.1.3 Solid Mechanics (solid)

Domains including Lithium Niobate substrate, Al electrodes and SiO2 insulator have been selected for *Solid Mechanics (solid)* physics, from which, Al electrodes and SiO2 insulator are *Linear Elastic Materials* and Lithium Niobate is *Piezoelectric Material*. Regarding mechanical boundary condition, bottom boundaries of Lithium Niobate substrate are fixed constraint ($u = 0$).

Material properties of LiNbO3 piezoelectric substrate including elasticity tensor (c_{ij}) coupling tensor (e_{ij}) and relative permittivity (ϵ_{ij}) are given in COMSOL material library [30]. These values are for z-cut, however one can use coordinate transformation, explained by Alud [33], to derive the values corresponded to 128 YX cut.

Another way to define crystal cut of a material in COMSOL, is to choose a coordinate system in the setting window of *Piezoelectric Material* node based on rotated system defined at *Definitions* interface, where Euler angles (α, β, γ) in COMSOL, see Figure 5-5, for 128 Y-X cut of Lithium Niobate in the 2D X-Y model are (0,270-38,0) in degree [34].

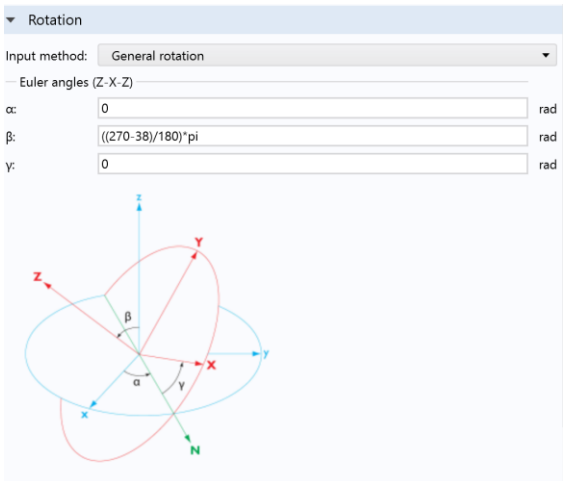

Figure 5-5 Setting Euler angles (α, β, γ) for Lithium Niobate 128 YX cut in Definitions interface of COMSOL.

5.2.1.4 *Electrostatics (es)*

Domains related to Piezoelectric substrate and SiO2 insulator are selected for *Electrostatics (es)* physics. Note that due to the higher electrical conductivity of Aluminium electrodes compared to Lithium Niobate and Silicon oxide, one can assume them as isopotential and consider only outer boundaries of such electrodes to indicate the type of its isopotential [27]. Silicon oxide insulator and Lithium Niobate piezoelectric substrate are selected for *Charge Conservation* and *Charge Conservation, Piezoelectric* interface respectively. Outer boundaries of Aluminium electrodes are selected for *Ground* and *Terminal* interfaces. Terminal type is voltage with $V_0 = 10V$.

5.2.1.5 *Pressure Acoustics, Frequency Domain (acpr)*

Domains related to PDMS layer and water microchannel are selected for Pressure Acoustics, Frequency Domain (acpr) physics. There are two nodes for pressure acoustics: *Pressure Acoustics 1* and *Pressure Acoustics 2*.

Pressure Acoustics 1 deals with acoustical features of water where fluid model is "thermally conducting and viscous" and corresponding fluid properties are given from material. Pressure Acoustics 2 includes PDMS layer where "user-defined attenuation" is chosen for fluid model. Attenuation length of acoustic waves in PDMS is equal to $12.8\,\lambda_{TSAW}$ [5].

In terms of fabrication, the sensor at the top side of microchannel, for quantifying microplastics, is supposed to be made of Polyethylene terephthalate (PET) material. Therefore, as it is shown in Figure 6-1, top layer of water microchannel has the PET acoustic impedance of $Z_n = 1370[kg/m^3] \times 2400[m/s]$.

5.2.1.6 *Laminar Flow (spf)*

Domain related to water microchannel is selected for *Laminar Flow (spf)* physics. Note that domains considered for PML at both sides cannot be selected for this physics. In the setting of *Laminar Flow (spf),* incompressible flow is chosen for compressibility that can be a valid assumption for microfluidics [1]. *P2+P1* is also chosen for discretization that considers higher-order interpolations for having more accuracy by saving cost-

effectiveness compared to other higher interpolations such as *P2+P2* or *P3+P3* [30, p. 1015].

Fluid properties such as density and viscosity are given from material. No slip wall condition is considered for the walls of microchannel. There is an inlet at left side and outlet at right side of microchannel. Normal inflow velocity v_{avr} is calculated from flow rate Q relation[1]:

$$Q = \int dy\, dz\, v_x(y,z) = A\, v_{avr} \qquad (6\text{-}2)$$

where for a typical flow rate of 250 $\frac{\mu L}{h}$ and cross section area of $A = w_m \times h_m = 500\mu m \times 110\mu m$, v_{avr} is calculated $1.26\,\frac{mm}{s}$.

5.2.1.7 Particle Tracing for Fluid Flow (fpt)

Particle Tracing for Fluid Flow (fpt) deals with the behavior of particles under the influence of different forces such as drag force and acoustic radiation force. Fluid domain is considered for this physics. For *Formulation* in the setting window of *Particle Tracing for Fluid Flow (fpt)*, one can choose *Newtonian, ignore inertial terms*, if the density of MPs would be close to fluid. Note that only in Newtonian formulation, forces related to gravity and buoyance can be introduced to the model. Walls of microchannel are assumed to be in freezing condition.

In the setting of *Particle Properties* node, particle density and diameter are chosen for *particle property specifications*. For 10 μm MPs, density is assumed $950\ kg/m^3$ which is close to density of Polyethylene, Polypropylene, and Polystyrene that are most abundant microplastics types observed in marine environment [35]. These values are presented in table 5-3 [12], [35].

In the acoustofluidics model, there are four main of forces affecting particle trajectory: Stokes drag force arising from acoustic streaming, acoustic radiation force arising from acoustic fields as well as gravitational and buoyant forces that are related to density of fluid and density and volume of particle. These four types of forces have been added to the model through Particle *Tracing for Fluid Flow (fpt)*.

Table 5-2*Microplastic properties used in the acoustofluidics COMSOL model*[12], [35].

Density ($\frac{kg}{m^3}$)	950
Diameter (µm)	10
Pressure-wave speed (m/s)	2400
Shear-wave speed (m/s)	1150

For the *Drag Force* interface, Stokes drag law has been selected for the setting of drag force[30], where velocity is obtained from *Velocity field (spf)* of *Laminar Flow (spf)* which is computed in the stationary study. For the *Acoustic Radiation Force* interface, *viscous* is selected for *Thermodynamic loss model* to consider the effect of viscosity in acoustic radiation force, which is discussed by Settnes and Bruus [12]. In *Acoustic Fields* tab, *Acoustic pressure* and *Acoustic velocity* are extracted from *Pressure Acoustics, Frequency Domain* physics which are computed in the frequency study. In *Particle Material Properties* tab, as an example, pressure wave and shear wave speeds of Polystyrene (PS) microplastics are used [12].

5.2.1.8 Multiphysics

Table 5-4 shows the Multiphysics used in the model with their corresponding coupled interfaces and domain/boundary.

Table 5-3 The list of different Multiphysics used for modelling the proposed acoustofluidics in COMSOL

Multiphysics	Coupled Interfaces	Domain/Boundary
Piezoelectric Effect	*Solid Mechanics (solid) Electrostatics (es)*	*Piezoelectric substrate domain*
Acoustic-Structure Boundary	*Pressure Acoustics (acpr) Solid Mechanics (solid)*	*Boundaries between insulator and PDMS*
Acoustic Streaming Domain Coupling	*Pressure Acoustics (acpr) Laminar Flow (spf)*	*Fluid domain*

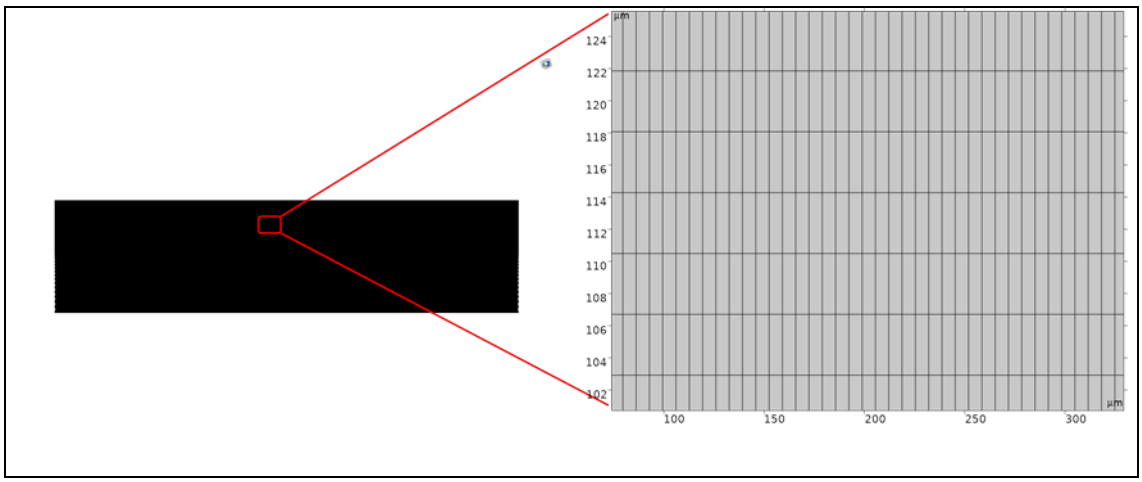

Figure 5-6 Rectangular mapped mesh of the acoustofluidics model with element sizes varying between $\frac{\lambda_{TSAW}}{13}$ *and* $\frac{\lambda_{TSAW}}{8}$*. One part of the mesh has been magnified. Units are in* μm*.*

5.2.1.9 Mesh

In order to have better control on meshing different domains as well as satisfying permissible mesh element size for acoustic domains, rectangular mapped mesh, as shown in Figure 5-6, has been implemented. For solving free-field wave problem, second order or quadratic elements size should be maximum one-fifth of wavelength ($h_{max} = \frac{\lambda_{TSAW}}{5}$) [36]. In the proposed model, the element size in acoustic domains varying between $\frac{\lambda_{TSAW}}{13}$ and $\frac{\lambda_{TSAW}}{8}$. Since the wave energy is mostly confined near the surface of substrate, for reducing simulation load, in the piezoelectric substrate, mesh size at the surface, $1.3\mu m \times 6.5\mu m$, are much finer than those ones near bottom, $20\mu m \times 6.5\mu m$.

5.2.1.10 Study

For simulating acoustic and stationary fields as well as particle trajectory of model, three different studies in *Frequency Domain*, *Stationery* and *Time Dependent* have been used which are described in the following.

Study 1: Acoustic field – Frequency Domain: In order to simulate acoustic fields such as acoustic pressure and velocity, frequency domain study has been used. In the setting of this study, frequency of 72.4 MHz is set which is the resonant frequency of the SAW resonator, see Figure 5-3. Based on the Figure of merit κ which is explained in chapter 4, at this frequency, 10 μm MPs particles can be translated effectively. Figure 5-7(a) shows the setting window of this study including different physics interfaces solved for the study.

Study 2: Stationery field – Stationery: For simulating stationary fields such as velocity of laminar flow and acoustic streaming, stationary study is utilized. As shown in Figure 5-7 (b), for reducing the computational cost of simulation, values of variable corresponded to study 1, frequency domain, is not solved again for stationary study.

Study 3: Particle Tracing – Time Dependent: This study deals with *Particle Tracing for Fluid Flow (fpt)* to simulate particles trajectories in time domain. In this study, values of variable corresponded to study 2, stationary, is not solved. The default time stepping setting, *Generalized alpha* method with strict steps taken by solver, has not been changed.

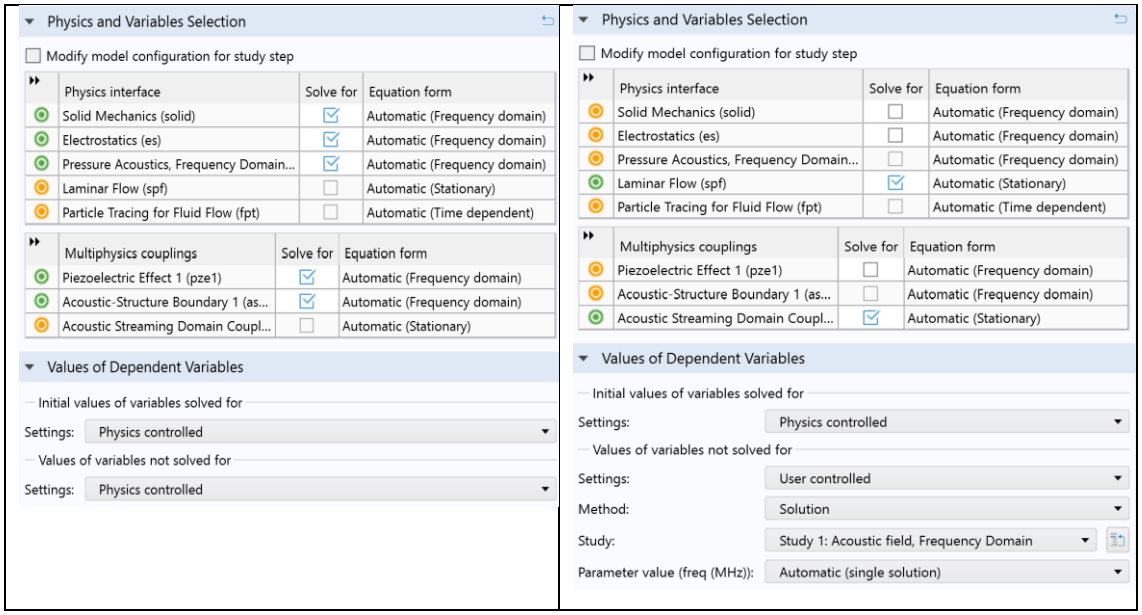

(a) (b)

Figure 5-7 Physics and variable selection tab with values of dependent variables considered for (a) frequency domain and (b) stationary fields studies setting

5.3 Simulation results

Herein, only some of the important simulation results of frequency domain and stationary studies which are used for computing particles trajectories, are presented and simulation results of time dependent study will be discussed in chapter 6.

Figure 5-8 (a) shows displacement field of piezoelectric substrate in *y*-direction from frequency domain study that has a maximum and minimum amplitude value of 1.2 nm. As shown in the picture, the displacement decays exponentially regarding the wavelength as wave propagates into the bulk of piezoelectric. Figure 5-8(b) is the total acoustic pressure in the microchannel at working frequency of 72.4 MHz from frequency domain study with actuation peak-to-peak voltage of 20V. The maximum acoustic pressure value is 0.86 MPa which gives acoustic energy density $E_{ac} = \frac{1}{2}\kappa_0 p_a^2 = 160\ J/m^3$ [12].

Figure 5-9 (a) and (b) also show total acoustic velocity (RMS) (m/s) from frequency domain study and velocity magnitude of laminar fellow (mm/s) from stationary fields study by considering acoustic streaming.

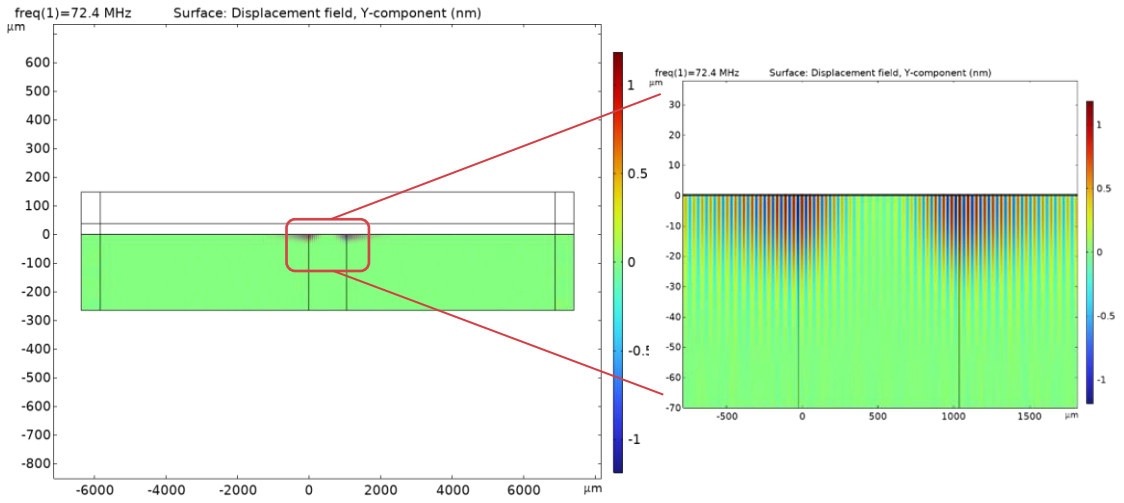

(a)

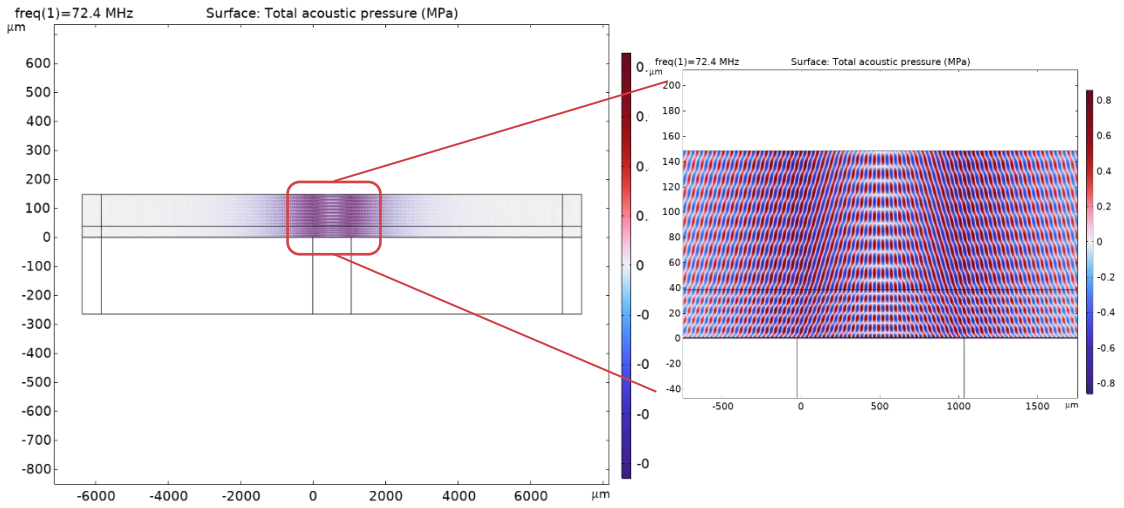

(b)

Figure 5-8 COMSOL simulation results corresponding to frequency domain study of the acoustofluidics model. (a) vertical displacement (nm) of piezoelectric substrate with maximum magnitude of 1.2 nm, (b) total acoustic pressure (MPa) in PDMS layer and water showing acoustic waves travelling to the left and right sides relative to the middle of microchannel. Maximum pressure is 0.86 MPa. Working frequency and peak-to-peak voltage are 72.4 MHz and 20V.(Y scale is 8 times larger than X scale.)

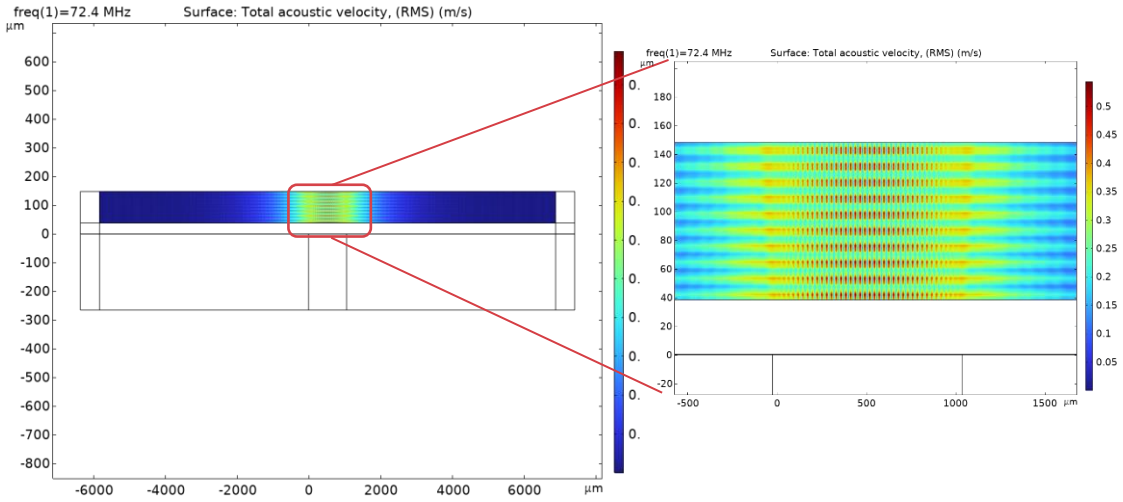

(a)

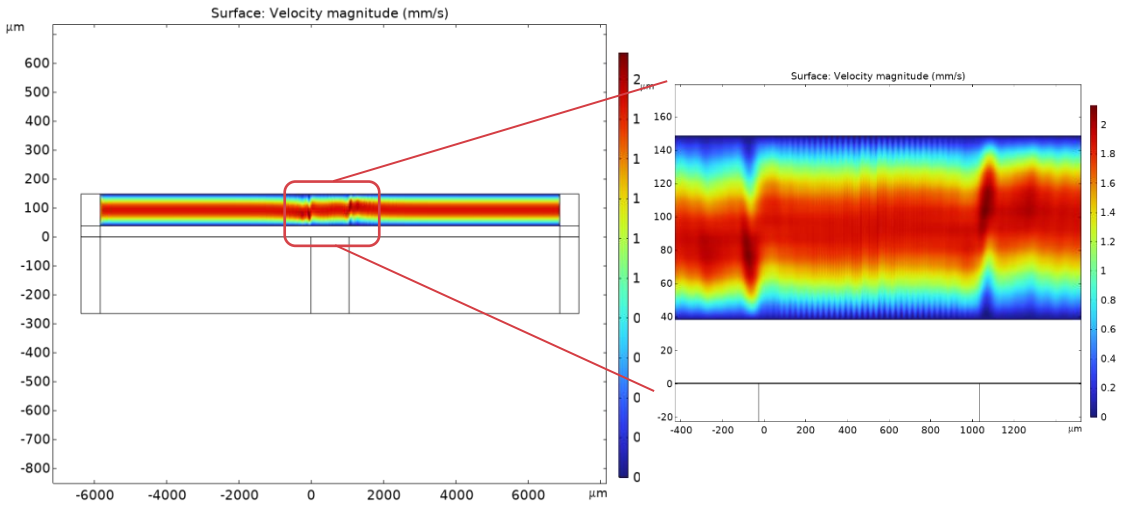

(b)

Figure 5-9 COMSOL simulation results corresponding to frequency domain and stationary fields study of the acoustofluidics model. (a) total acoustic velocity (RMS) (m/s) in the microchannel, (b) velocity magnitude (m/s) of fluid with normal inflow velocity of 1.26 mm/s by considering acoustic streaming. Working frequency and peak-to-peak voltage are 72.4 MHz and 20V. (Y scale is 8 times larger than X scale.)

6 Simulating microplastics trajectories in COMSOL

The literature review carried out during doing this project showed that there is a lack of numerical simulations of acoustophoresis driven by travelling surface acoustic waves (TSAWs) in the scientific literatures. It is important to predict the trajectories of microparticles in the microchannel with presence of acoustic fields, before proceeding with fabrication process that could be costly and time consuming.

This chapter deals with the equation COMSOL uses to calculate the acoustic radiation force (ARF), followed by introducing a new permissible equation for ARF in acoustic travelling wave, which is used for the first time, instead of main COMSOL equation to calculate the particle trajectories correctly. Finally, the simulation results for different microplastics and driving conditions have been presented.

6.1 Acoustic radiation force in COMSOL

As it is shown in the equation tab located in the setting of the *Acoustophoretic Radiation Force* interface, COMSOL uses the following equation, presented also in chapter 4, for calculating ARF for both standing and travelling waves:

$$\boldsymbol{F}^{rad} = -\pi a^3 \left[\frac{2\kappa_0}{3} Re[f_1^* p_{in}^* \nabla p_{in}] - \rho_0 Re[f_2^* \boldsymbol{v}_{in}^* . \nabla \boldsymbol{v}_{in}]\right] \qquad (6\text{-}1)$$

Where $\boldsymbol{p_{in}}$ and $\boldsymbol{v_{in}}$ are incoming pressure and velocity acoustic fields evaluated at $r = 0$ [12]. Details on how to derive this equation from scattering and perturbation theory, can be found in references [12], [22].

Figure 6-1 shows the trajectories of 10 μm Polystyrene (PS) microplastics particles, simulated in the proposed acoustofluidics model, see Figure 5-4, through main ARF equation in COMSOL, equation (6-1). As shown in this diagram, when particles approach to the high-pressure zone near the IDT, they stop at the middle of microchannel, while, due to the y-component of travelling acoustic radiation force, they can be displaced towards ceiling of microchannel.

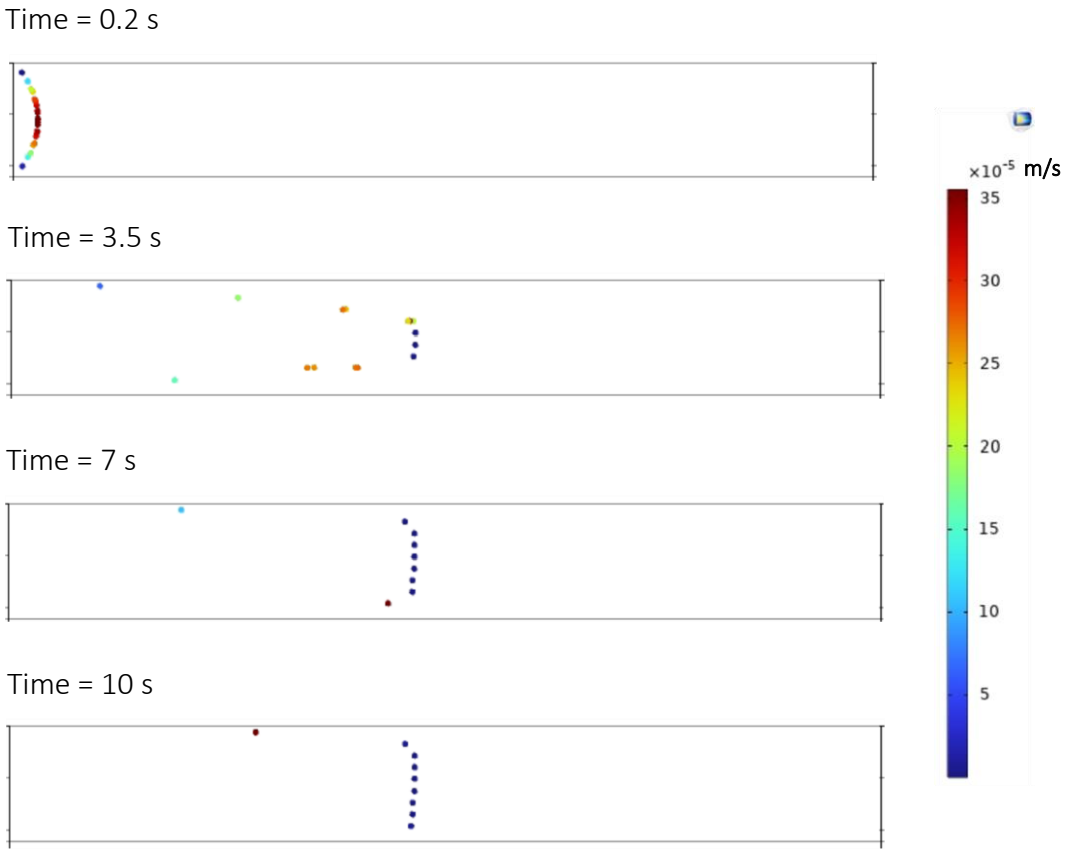

Figure 6-1 COMSOL simulation of 10 μm Polystyrene particles trajectories in the microchannel of proposed acoustofluidics model in different times of t= 0.2, 3,5, 7, and 10 s. Colors show velocity of microparticles in m/s.

The simulated particle trajectories are different from the behaviour of microparticles under influence of travelling acoustic waves reported experimentally in the papers. For example, Destgeer et al. have shown size-selective separation of 3, 5, and 7 μm by means of slanted interdigitated transducer (SIDTS) generating tunable travelling surface acoustic waves [6].

6.2 Driving acoustic radiation force of a travelling wave

As Bruus shows in [12], an incoming travelling wave $f(r,t)$ can be expressed in the form $f(r)e^{i(\omega t+kr)}$ where ω is angular frequency and k is wave number. Despite standing wave, travelling wave has a phase changing plane-wave factor e^{ikr} contributing in

radiation force [12]. Travelling acoustic pressure and velocity waves are represented in equations (6-2).

$$p_{in} = |p_{in}|e^{i(\omega t+kr)} \quad (6\text{-}2a)$$

$$\boldsymbol{v}_{in} = |\boldsymbol{v}_{in}|e^{i(\omega t+kr)} \quad (6\text{-}2b)$$

$$f_1 = f_1^{re} + if_1^{imag} \quad (6\text{-}2c)$$

$$f_2 = f_2^{re} + if_2^{imag} \quad (6\text{-}2d)$$

where, $i^2 = -1$ and p_{in} and $\boldsymbol{v}_{in}$ are incoming travelling acoustic pressure and velocity waves with the amplitude $|p_{in}|$ and $|\boldsymbol{v}_{in}|$ and f_1 and f_2 are monopole and dipole scattering coefficient. Note that amplitude of incoming plane waves $|p_{in}|$ and $|\boldsymbol{v}_{in}|$ are assumed to be constant for planar wave.

By substituting equations (6-2a) to (6-2d) in the main acoustic radiation force equation (6-1), one can obtain:

$$\begin{aligned}\boldsymbol{F}^{rad} &= -\pi a^3\left[\frac{2\kappa_0}{3}Re[f_1^* p_{in}^* \nabla p_{in}] - \rho_0 Re[f_2^* \boldsymbol{v}_{in}^*.\nabla \boldsymbol{v}_{in}]\right] \\ &= -\pi a^3\left[\frac{2\kappa_0}{3}Re\left[(f_1^{re} - if_1^{imag})|p_{in}|e^{-i(\omega t+kr)}ik|p_{in}|e^{i(\omega t+kr)}\right]\right. \\ &\left. - \rho_0 Re\left[\left(f_2^{re} - if_2^{imag}\right)|\boldsymbol{v}_{in}|^2 e^{-i(\omega t+kr)}\nabla e^{i(\omega t+kr)}\right]\right] \\ &= -\pi a^3\left[\frac{2\kappa_0}{3}Re\left[(f_1^{re} - if_1^{imag})ik|p_{in}|^2\right]\right. \\ &\left. - \rho_0 Re\left[\left(f_2^{re} - if_2^{imag}\right)ik|\boldsymbol{v}_{in}|^2\right]\right]\end{aligned} \quad (6-3)$$

Based on the above equations, the resulting acoustic radiation force of a travelling acoustic waves is:

$$\boldsymbol{F}^{rad} = -\pi a^3\left[\tfrac{2\kappa_0}{3}f_1^{imag}|p_{in}|^2 - \rho_0 f_2^{imag}|\boldsymbol{v}_{in}|^2\right]\boldsymbol{k} \quad (6\text{-}4)$$

where, $\boldsymbol{k} = k_x e_x + k_y e_y$ is parallel to $\boldsymbol{v}_{in}$.

Since monopole scattering coefficient f_1 is real-valued[12], equation (6-4) can be more simplified into:

$$\boldsymbol{F}^{rad} = \pi a^3 \rho_0 f_2^{imag} |\boldsymbol{v}_{in}|^2 \boldsymbol{k} \qquad (6\text{-}5)$$

The expression for equation (6-4) which is introduced to COMSOL is given in appendix.

6.2.1 Driving wave number from acoustic pressure

As acoustic waves on surface of Lithium Niobate are generated, they couple into fluid with a specific propagation angle which, based on the Snell's law, is proportional to the ratio of acoustic impedance of substrate and fluid [6].

One way to derive wavenumber $\boldsymbol{k} = k_x e_x + k_y e_y$ of a travelling acoustic wave is to measure the corresponding wavelength along X and Y axis. Figure 6-2(a) and (b) shows total acoustic pressure (Pa) along horizontal and vertical cutlines plotted in water acoustic domain.

Based on this Figure, wavenumber along X axis $k_x = \frac{2\pi}{\lambda_x} = 115.6\, mm^{-1}$ and along Y axis $k_y = \frac{2\pi}{\lambda_y} = 277.9\, mm^{-1}$ are calculated. Accordingly, the angle of propagation relative to vertical axis can be calculated by $\theta = \tan^{-1}\frac{k_x}{k_y} \approx 22.6^{\circ}$.

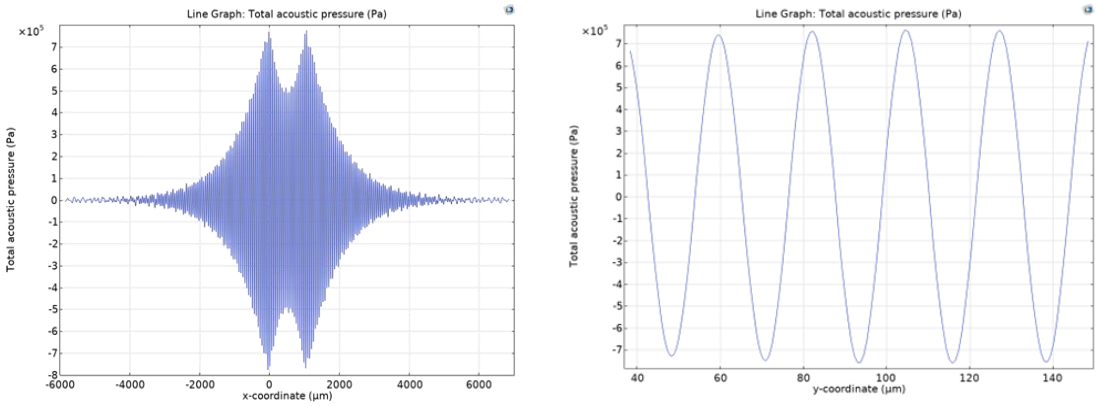

(a) *(b)*

Figure 6-2 Total acoustic pressure along (a) horizontal cutline and (b) vertical cutline plotted in water acoustic domain

6.3 Validating COMSOL model by an example

In order to validate the COMSOL model with new equation (6-4) for travelling ARF instead of equation (6-1), it is evaluated by an example solved by Settnes and Bruus [12]. They assume a planar travelling wave with $\boldsymbol{k} = ke_z$ and $p_1 = p_a e^{i(kz-\omega t)}$ having a typical acoustic energy density $E_{ac} = \frac{1}{2}\kappa_0 p_a^2$ equal to $100\, J/m^3$. The acoustic radiation force formula based on acoustic energy density is derived by equation (7-6)[12].

$$\boldsymbol{F}^{rad} = \pi a^3 k f_2^i(\tilde{\rho}, \tilde{\delta}) E_{ac} e_z \qquad (6\text{-}6)$$

In this example, Pyrex sphere microparticles with radius $a = 2.5\ \mu m$ are in water with frequency $f = 1.5\ MHz$. In this case one can obtain: $\tilde{\delta} = 0.18$, $k = 6.36 \times 10^3 m^{-1}$, $\tilde{\rho} = 2.23$ and $f_2^i(2.23, 0.18) = 0.05$. By substituting these values in equation (6-6) acoustic radiation force will be $F^{rad} = 1.46\ pN$. Note that some values like k and $f_2^i(\tilde{\rho}, \tilde{\delta})$ in the example provided by reference [12] has been corrected.

Figure 6-3 (a) and (b) show total acoustic pressure (Pa) and total acoustic velocity (RMS) (m/s) of the microchannel simulated in COMSOL to investigate introducing equation (6-4) for travelling ARF to COMSOL. It is a water-filled rectangular microchannel with dimension $W \times H = 3800 \times 1272\ \mu m^2$. In this model, $\boldsymbol{k} = ke_x$, see Figure 6-3(a).

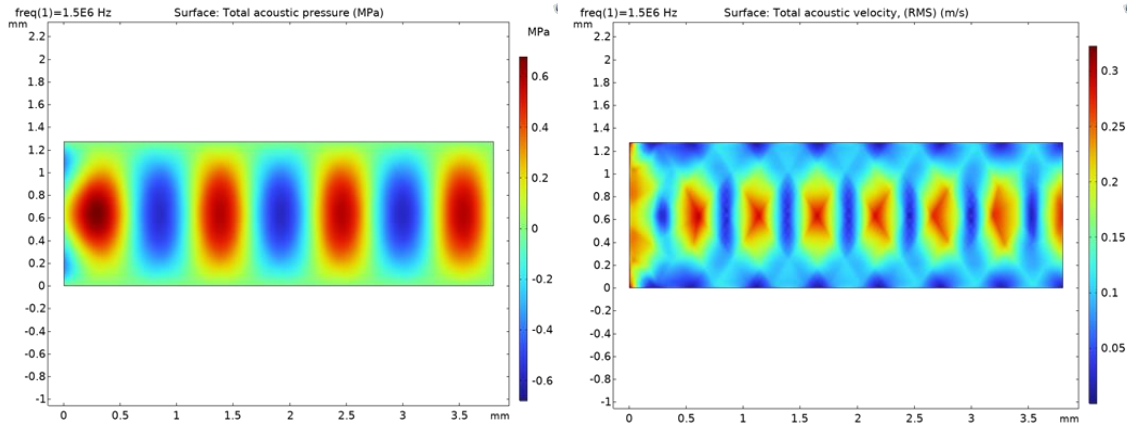

(a) *(b)*

Figure 6-3 *(a)Total acoustic pressure (Pa) and (b) total acoustic velocity (RMS) (m/s) of the microchannel simulated in COMSOL to validate new equation introduced to COMSOL for computing ARF from acoustic travelling wave.*

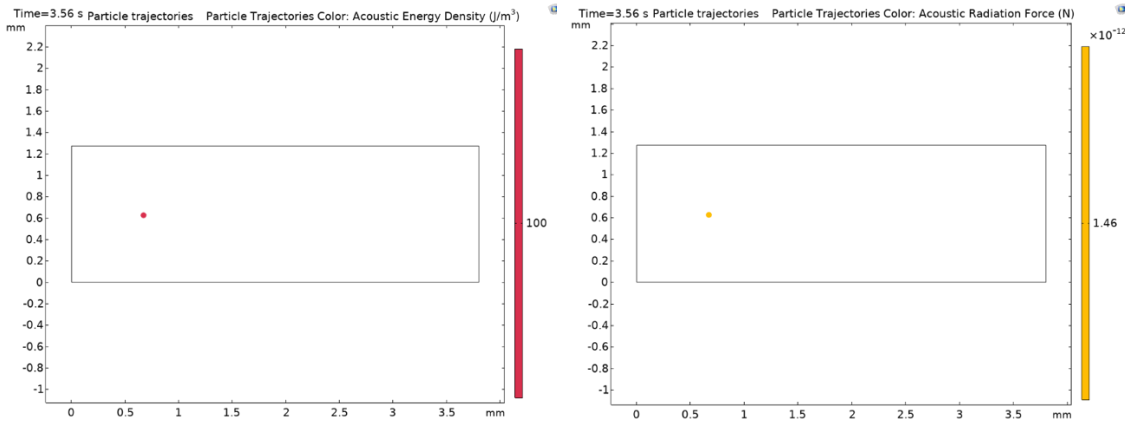

(a) *(b)*

Figure 6-4 (a) Acoustic energy density $E_{ac} = 100\ J/m^3$ and (b) travelling acoustic radiation force on 5 μm diameter Pyrex particle at time=3.56 s, $\boldsymbol{F}^{rad} = 1.46\ pN$

In this model, left boundary is a *Thermoviscous Boundary Layer Impedance* vibrating with velocity $d_0\omega$ where $f = 1.5\ MHz$ and d_0 has set to 30 nm to induce acoustic energy density equals to 100 J/m^3. Other boundaries are considered sound soft ones.

A 5 μm diameter Pyrex particle is placed firstly in coordination $(q_x, q_y) = (0.5mm, 0.625mm)$ through *Release from Grid* node from *Particle Tracing for Fluid Flow (fpt)* physics. Since the only force exerted on particle is acoustic radiation force in x direction, the particle moves along this direction and after Time=3.56 s, the particle reaches the area where acoustic energy density equals to 100 J/m^3 , see Figure 6-4(a). At this point, acoustic radiation force $\boldsymbol{F}_x^{rad}$ equals to 1.46 pN, see Figure 6-4 (b). The acoustic radiation force from simulation is the same with the value calculated by Settnes and Bruus [12].

6.4 Characterization of the proposed acoustofluidics model

This section deals with characterization of the proposed acoustofluidics model and investigation of particles trajectories through changing microplastics size and density as well as voltage, normal inflow velocity and frequency of SAW resonator through evaluating these changes effects on the particle trajectories simulated in COMSOL.

6.4.1 Microplastics size

Based on equation (6-5), the acoustic radiation force is proportional to the cubic of particles radius ($\boldsymbol{F}^{rad} \propto a^3$). Therefore, microplastics size play an effective role in amplitude of ARF so that submicron microplastics hardly scattered by acoustic waves.

Figure 6-5 shows spherical microplastics trajectories with diameters 0.7, 3, 7, 10, 15 and 25 μm. The density of all particles is the same and equal to 920 kg/m^3 which is close to density of Polyethylene and Polypropylene, materials used for plastic bags and rope, for example, which are also two most common types of microplastics found in marine environment [35]. For each case, 20 uniformly distributed particles are released from the inlet located on the left side of microchannel and due to the drag force move towards outlet at right side of microchannel. The microchannel in this Figure is extended in range of [-5855µm,6865µm] on X-axis and [38µm,148µm] on Y-axis. The particles trajectories are computed based on formulation *Newtonian, ignore inertial terms*. Actuation voltage of SAW resonator $V_{p-p} = 20\,V$ and normal inflow velocity $U_0 = 1.26\,mm/s$ remained the same for simulation of all particle trajectories. Table 6-1 shows the percentage of MPS for each group trapped on the ceiling of microchannel with coordination of such particles.

Table 6-1 Effect of ARF on microplastics with different size based on COMSOL simulation results.

Diameter (μm)	Percent of MPS trapped by ARF on ceiling (%)	Y coordination (μm)	X coordination (mm)
0.7	0	-	-
3	10	> 130 µm	[0,1]
7	25	> 115 µm	[-0.4,1.8]
10	30	> 110 µm	[-0.4,1]
15	50	> 95 µm	[-0.8,1.5]
25	80	> 70 µm	[-1,1.5]

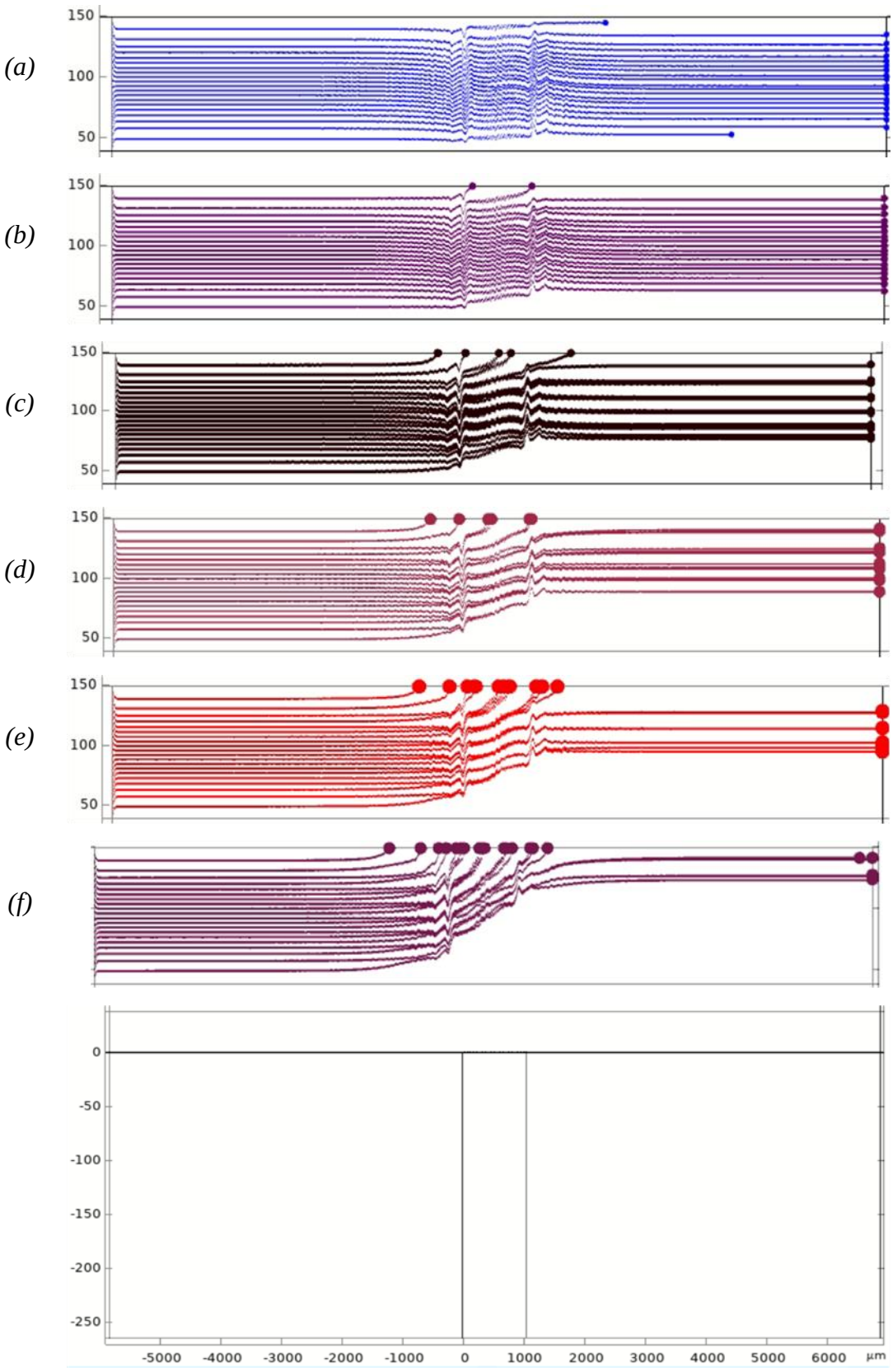

Figure 6-5 Microplastics trajectories with diameters of (a) 0.7 µm, (b) 3 µm, (c) 7 µm, (d) 10 µm, (e) 15 µm, and (f) 25µm in the microchannel.

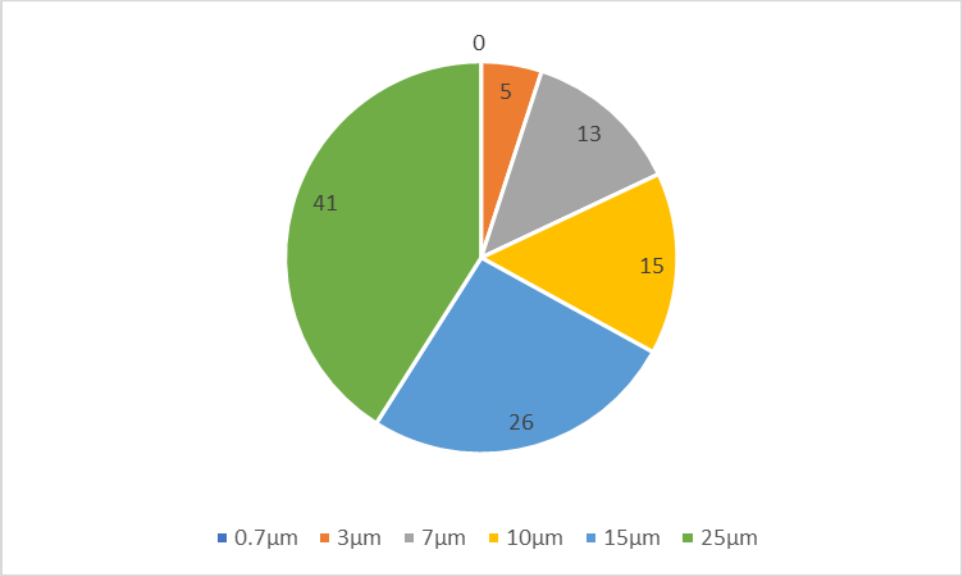

Figure 6-6 Percentage of MPs with different size trapped on the top of microchannel.

Figure 6-6 shows the distribution of MPs with different size trapped on the ceiling of microchannel with the percentage of each group. Based on above Figures and table, by increasing microplastics size, more microplastics distributed along Y-axis is affected by ARF which results in higher percentage of bigger microplastics compared to smaller ones accumulated on the ceiling.

6.4.2 Microplastics density

Table 6-2 from reference [35] shows the application and density of most abundant microplastics observed in marine environment. Most of these plastics have density close to the water. This section deals with the effect of MPs density on ARF.

Based on the equation for imaginary part of dipole scattering coefficient f_2 which is discussed in chapter 4, rewritten again below, this scattering coefficient which is attributed to translational motion of particles is related to the density ratio of particle and fluid.

$$f_2^i(\tilde{\rho},\tilde{\delta}) = Im[f_2(\tilde{\rho},\tilde{\delta})] = \frac{6(1-\tilde{\rho})^2(1+\tilde{\delta})\tilde{\delta}}{(1+2\tilde{\rho})^2+9(1+2\tilde{\rho})\tilde{\delta}+\frac{81}{2}(\tilde{\delta}^2+\tilde{\delta}^3+\frac{1}{2}\tilde{\delta}^4)} \qquad (6\text{-}7)$$

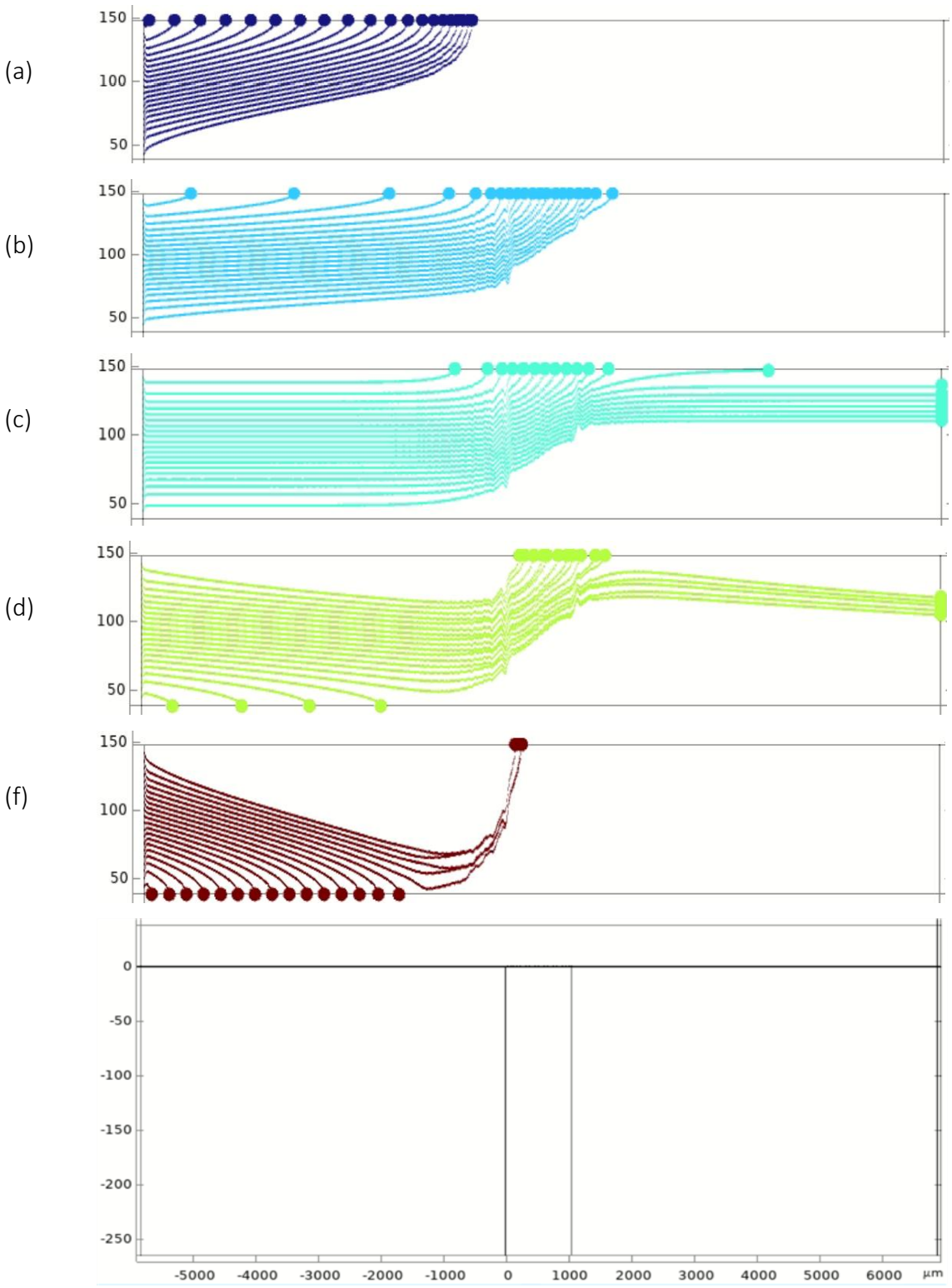

Figure 6-7 $10\ \mu m$ microplastics trajectories with different density of (a)700 kg/m^3, (b) 950 kg/m^3, (c) 1030 kg/m^3, (d)1150 $kg/m^3$and (f)1500 kg/m^3.

By making the density of microplastics equal to fluid, based on equation (6-5) and (6-7), because f_2^i vanishes when $\tilde{\rho} = 1$, the travelling acoustic radiation force would be zero.

Table 6-2 *Application and density of most abundant microplastics observed in marine environment* [35]

MPs material	Applications	Density $\times 10^3$ (kg/m^3)
Polyethylene	Plastic bags, storage containers	0.91–0.95
Polypropylene	Rope, bottle caps, gear, strapping	0.90–0.92
Polystyrene (expanded)	Cool boxes, floats, cups	0.01–1.05
Polystyrene	Utensils, containers	1.04–1.09

Figure 6-7 shows 10 µm microplastics trajectories with different density of 700, 950, 1030, 1150 and 1500 kg/m^3. Density of water is assumed $\rho_0 = 1030\ kg/m^3$ which is close to density of sea water[31]. Here, the particle trajectories are computed with Newtonian formulation ($\frac{d(m_P v)}{dt} = F_t$) where buoyant and gravitational forces are also considered in the model. The voltage V_{p-p} of SAW resonator and normal inflow velocity are 20V and 1.26 mm/s.

Based on Figure 6-7, particles having much lower, see Figure 6-7(a), and higher, see Figure 6-7(f), density than water are affected largely by buoyant and gravitational forces, resulting in floating and sinking, respectively, in the water before reaching above IDT and being affecting by ARF. In Figure 6-7(c), density of microplastics is equal to water and they do not experience travelling acoustic radiation forces. Therefore, as it is shown in the Figure 6-8, these suspended microplastics follow only the streamline. In this Figure black and turquoise lines show streamline and microplastics trajectories respectively.

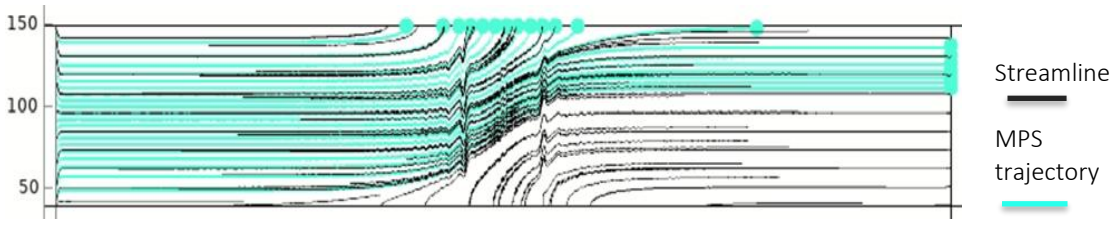

Figure 6-8 *Trajectories of MPs with the same density with water and streamline in the microchannel. In this case, MPs follow the streamline.*

6.4.3 Actuation voltage of SAW resonator

Increasing the actuation voltage of SAW resonator causes an increment in acoustic pressure amplitude p_a(Pa) resulting in higher acoustic energy density $E_{ac} = \frac{1}{2}\kappa_0 p_a^2$.

For example, by increasing peak-to-peak voltage from 14 V to 30V, maximum total acoustic pressure in the microchannel is increasing from 0.6 MPa to 1.2 MPa respectively. Therefore, it is expected that by increasing the input voltage, more microplastics be concentrated on the ceiling of microchannel.

Figure 6-9 shows the simulated 10 μm MPs trajectories in three different peak-to-peak voltages of 14, 20, and 30 V. MPs density is 950 kg/m^3 and normal inflow velocity is equal to 0.6 mm/s and constant for three cases. As shown in this Figure, for voltages below 20 V, when MPs reach above IDT, due to the travelling ARF, they are deflected upwards, however, the force $\boldsymbol{F}^{rad}$ is not big enough to overcome Stokes drag force $\boldsymbol{F}^{drag}$ and only a few of them having lower velocity and are close to the ceiling can be pushed to the ceiling . Equation (6-8) shows Stokes drag force which is proportional to the streaming velocity and particle radius.

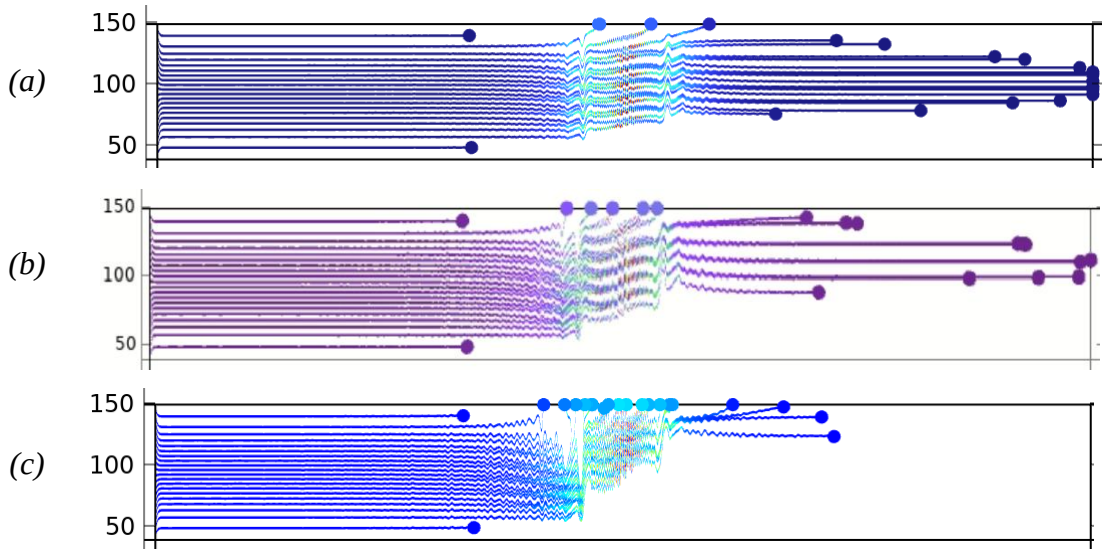

Figure 6-9 10 μm MPs trajectories with different actuation voltage V_{p-p}(a) 14V,(b) 20V, and (c) 30V. MPs density and normal inflow velocity are 950 kg/m^3 and to 0.6 mm/s.

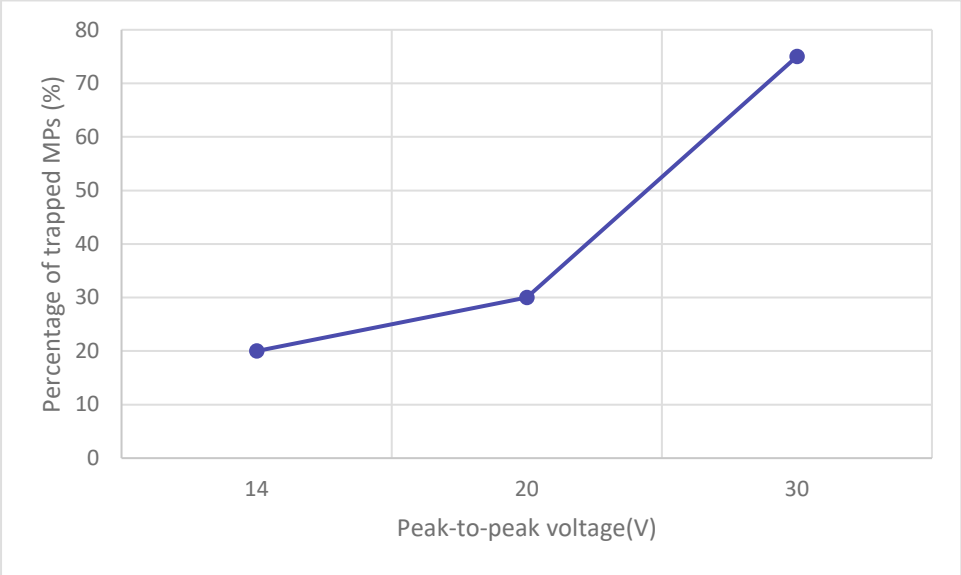

Figure 6-10 Percentage of 10 μm MPs with density of 950 kg/m^3 which are trapped on the ceiling, above IDT, versus the applied peak-to-peak voltage

$$\boldsymbol{F}^{drag} = 6\pi\eta a\left(\boldsymbol{v}_2 - \boldsymbol{v}_p\right) \qquad (6\text{-}8)$$

where η and $\boldsymbol{v}_2$ are fluid viscosity and streaming velocity as well as a and $\boldsymbol{v}_p$ are particle radius and velocity.

As shown in Figure 6-9, by increasing voltage from 14V to 30V, more MPs are trapped on the ceiling of microchannel. Figure 6-10 also shows the diagram of percentage of MPs trapped on the ceiling above IDT according to the input voltage.

6.4.4 Normal inflow velocity

By neglecting gravitational and buoyant forces, two main forces of Stokes drag force and acoustic radiation force can determine the MPs trajectories. For trapping MPs on the ceiling of microchannel, travelling ARF should be equal to Stokes drag force.

$$6\pi\eta a\left(\boldsymbol{v}_2 - \boldsymbol{v}_p\right) = \pi a^3 k f_2^i(\tilde{\rho}, \tilde{\delta}) E_{ac} \qquad (6\text{-}9)$$

In equation 6-9, streaming velocity is proportional to the normal inflow velocity.

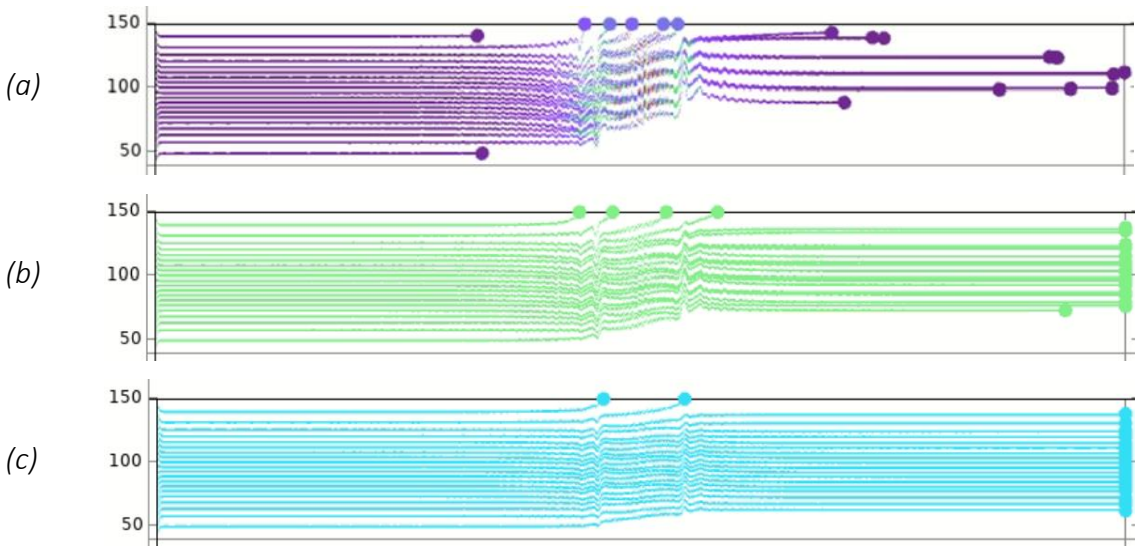

Figure 6-11 10 μm MPs trajectories with different normal inflow velocity of (a) 0.6 mm/s, (b) 1.2 mm/s, and (c) 2.4 mm/s. MPs density and applied peak-to-peak voltage are 950 kg/m^3 and 20V.

Figure 6-11 shows that by increasing normal inflow velocity from 0.6 mm/s to 2.4 mm/s more MPs escape from IDT region due to overcoming Stokes drag force to the travelling acoustic radiation force. Particles that are close to top of microchannel, due to experiencing lower Stokes drag force because of having lower velocity, can be pushed up to the ceiling.

6.4.5 Working frequency

The frequency of SAW resonator is another important parameter playing role in the particle trajectories of MPs. As it is discussed in chapter 4, the Figure of merit $\kappa = \frac{2\pi}{\lambda} a$ is an important parameter for microparticles with radius a to be affected by acoustic fields with wavelength λ.

For example, for Polystyrene microplastics, κ should be greater than 1.3 [4]. Therefore, for MPs with radius 5 μm, the frequency of acoustic fields should be greater than 62 MHz, the sound velocity in water is assumed 1500 m/s.

Figure 6-12 shows 10 μm MPs trajectories with density of 950 kg/m^3 in three different frequencies of 36.2, 72.4 and 144 MHz. The voltage V_{p-p} and normal inflow velocity are constant and equal to 20 V and 1.26 mm/s.

As shown in Figure 6-12, for the frequency 36.2 MHz, 10 µm MPs pass the length of microchannel without being affected by acoustic radiation force or streaming. By increasing the frequency to 72.4 MHz, acoustic radiation force can deflect the flow of MPs when they reach above the IDT or high-pressure zone. In frequency of 144 MHz, through increasing ARF, more MPs are trapped above IDT.

As shown in the Figure, magnitude of total acoustic radiation force (N) for three frequencies of 36.2, 72.4 and 144 MHz are in order of 10^{-14}, 10^{-13}, and 10^{-12} showing increasing the frequency by as much as two times results in an increment in acoustic radiation force of up to ten times.

(a)

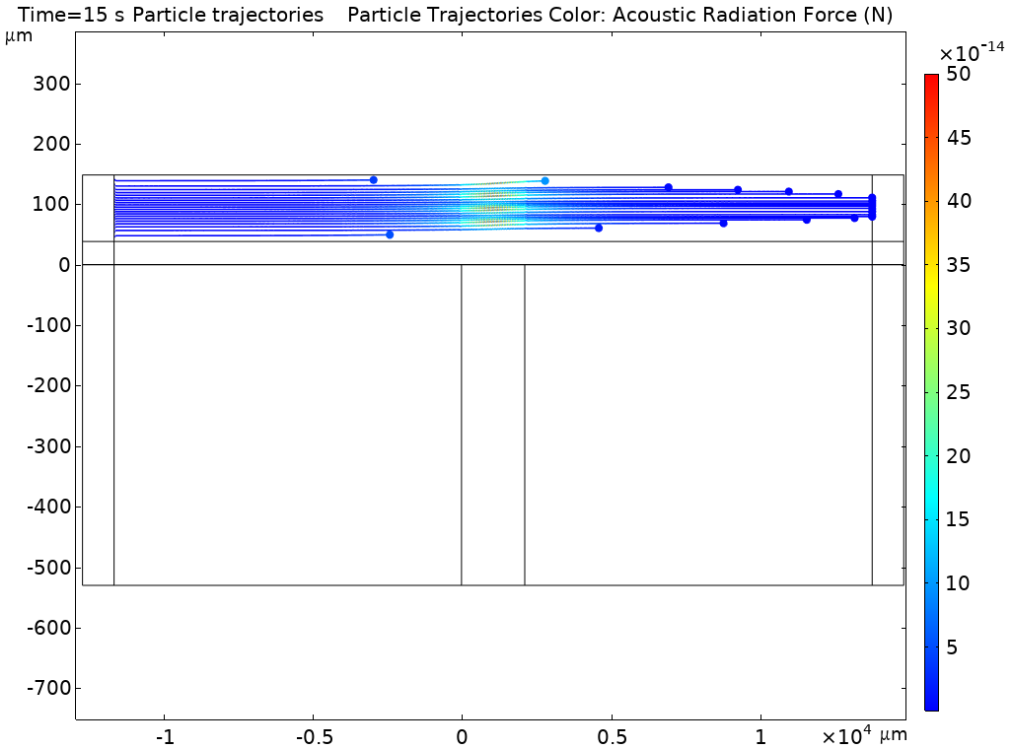
Time=15 s Particle trajectories
Particle Trajectories Color: Acoustic Radiation Force (N)
μm
300
200
100
0
-100
-200
-300
-400
-500
-600
-700
-1
-0.5
0
0.5
1
×10^4 μm
×10^-14
50
45
40
35
30
25
20
15
10
5

(b)

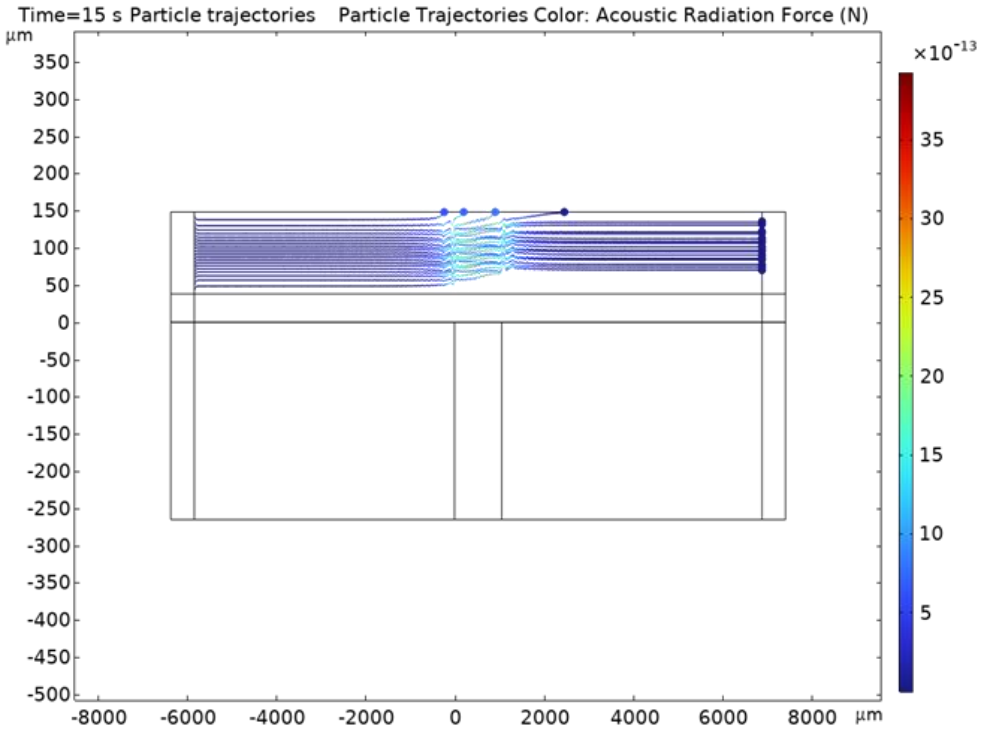
Time=15 s Particle trajectories
Particle Trajectories Color: Acoustic Radiation Force (N)
μm
350
300
250
200
150
100
50
0
-50
-100
-150
-200
-250
-300
-350
-400
-450
-500
-8000
-6000
-4000
-2000
0
2000
4000
6000
8000
μm
×10^-13
35
30
25
20
15
10
5

(c)

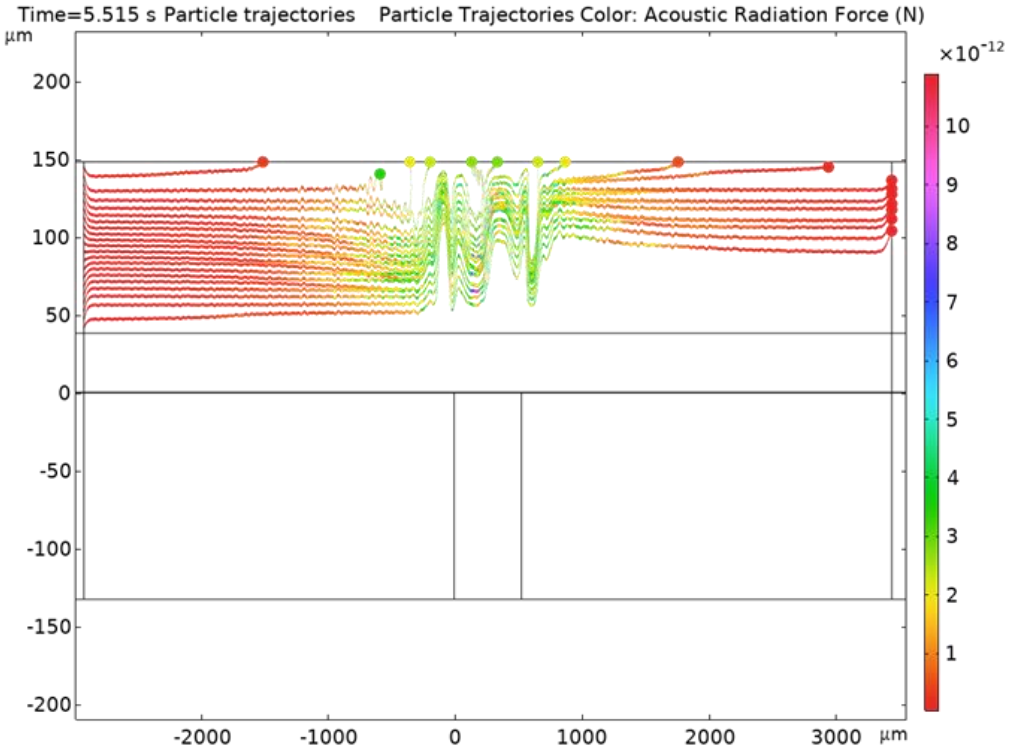

Figure 6-12 10 µm MPs trajectories with different acoustic field frequencies of (a) 36.2 MHz, (b) 72.4 MHz, and (c) 144 MHz. Trajectory colors represent the total acoustic radiation force (N). Normal inflow velocity and applied peak-to-peak voltage are 1.26 mm/s and 20V.

7 Discussion

This master thesis has been inspired by the paper "Microparticle self-assembly induced by travelling surface acoustic waves" written by Destgeer et al. [5]. In their acoustofluidics model, there is a TSAW resonator beneath a microchannel to push 10 µm Polystyrene microparticles to the ceiling of microchannel. This technique can be used in the self-assembly process based on which any cracks and defects in a lattice structure can be repaired [5]. Although the simulation results provided in this master thesis is in good consistent with the experimental work of the mentioned paper, there are some differences, particularly in peak-to-peak actuation voltage of TSAW resonator in the paper with the model in COMSOL.

For example, they could accumulate the Polystyrene microparticles with density of 1050 kg/m^3 on top of microchannel by minimum voltage V_{p-p} of 4.2 V with flow rate of 250 µL/h, however they have not reported how many percentages of microparticles are trapped in this case. In the model simulated in COMSOL, with normal inflow velocity of 1.26 mm/s which is correspond to flow rate of 250 µL/h for the same microchannel dimension $W \times H = 500\mu m \times 110\mu m$, only 20 percent of MPs with density of 950 kg/m^3 could be accumulated on top of microchannel. However, the simulation results are based on travelling acoustic radiation force discussed by Settnes and Bruus [12] where by approaching the density of MPs to the fluid, $\tilde{\rho} = 1$, the acoustic radiation force provoked by travelling waves could be vanished.

The second discussion is about numerical simulation of acoustofluidics model with travelling surface acoustic waves. Most of the numerically simulated models presented in the literatures are based on acoustic standing waves in the microchannel. For example, the model for "Acoustic Streaming in a Microchannel Cross Section" available in the application libraries of COMSOL 6.1 [26], deals with acoustic radiation force and streaming in a microchannel with standing waves. Therefore, the only reliable example that could be found to evaluate the simulation results based on the formula for travelling ARF, is the analytical example for calculating travelling ARF provided by Settnes and Bruus [12].

8 Conclusion

In this thesis, an acoustofluidics model was designed and simulated in COMSOL finite element model software. This model can be used to trap microplastics (MPs) with a typical size of 10 μm and density of 950 kg/m^3. One of the main applications of this model could be in quantifying MPs in marine environment.

Some of the necessary governing equations of microfluidics and acoustofluidics for driving acoustic radiation force (ARF) were provided in chapter 2 and 3. All the steps of modelling in COMSOL were discussed in chapter 5 with details so that it can also be used as a tutorial for modeling acoustofluidics. At the end of this chapter, some of the important simulation results such as mechanical displacement, total pressure and velocity acoustic, and velocity magnitude of laminar flow from frequency domain and stationary fields studies were presented.

The model, which was simulated based on ARF for travelling wave, was characterized in chapter 6 to investigate the MPs trajectories with different size and density as well as driving conditions such as normal inflow velocity, voltage, and frequency of travelling surface acoustic waves resonator. It has been shown that by choosing appropriate flow rate, voltage and frequency, the MPs with diameters bigger than 7 μm and density of 950 kg/m^3 can be trapped on the ceiling of microchannel above the TSAW resonator.

Regarding future works, a model based on the simulation results can be fabricated to compare COMSOL simulation results provided in this project with values derived from experiments. The model is also capable of employing a sensor on the ceiling of microchannel, where MPs are accumulated, to measure the number of MPs in a sample. The appropriate technique that can be used to sense such microparticles on top of a PDMS microchannel could be another topic for future works.

References

[1] H. Bruus, “Acoustofluidics 1: Governing equations in microfluidics,” *Lab. Chip*, vol. 11, no. 22, p. 3742, 2011, doi: 10.1039/c1lc20658c.

[2] M. Wu, A. Ozcelik, J. Rufo, Z. Wang, R. Fang, and T. Jun Huang, “Acoustofluidic separation of cells and particles,” *Microsyst. Nanoeng.*, vol. 5, no. 1, p. 32, Jun. 2019, doi: 10.1038/s41378-019-0064-3.

[3] X. Ding *et al.*, “Cell separation using tilted-angle standing surface acoustic waves,” *Proc. Natl. Acad. Sci.*, vol. 111, no. 36, pp. 12992–12997, Sep. 2014, doi: 10.1073/pnas.1413325111.

[4] D. J. Collins, Z. Ma, J. Han, and Y. Ai, “Continuous micro-vortex-based nanoparticle manipulation via focused surface acoustic waves,” *Lab. Chip*, vol. 17, no. 1, pp. 91–103, Dec. 2016, doi: 10.1039/C6LC01142J.

[5] G. Destgeer, A. Hashmi, J. Park, H. Ahmed, M. Afzal, and H. J. Sung, “Microparticle self-assembly induced by travelling surface acoustic waves,” *RSC Adv.*, vol. 9, no. 14, pp. 7916–7921, 2019, doi: 10.1039/C8RA09859J.

[6] G. Destgeer, B. H. Ha, J. Park, J. H. Jung, A. Alazzam, and H. J. Sung, “Microchannel Anechoic Corner for Size-Selective Separation and Medium Exchange via Traveling Surface Acoustic Waves,” *Anal. Chem.*, vol. 87, no. 9, pp. 4627–4632, May 2015, doi: 10.1021/acs.analchem.5b00525.

[7] H. Wang *et al.*, “Modelling hybrid acoustofluidic devices for enhancing Nano- and Micro-Particle manipulation in microfluidics,” *Appl. Acoust.*, vol. 205, p. 109258, Mar. 2023, doi: 10.1016/j.apacoust.2023.109258.

[8] H. Bruus, “Acoustofluidics 2: Perturbation theory and ultrasound resonance modes,” *Lab Chip*, vol. 12, no. 1, pp. 20–28, 2012, doi: 10.1039/C1LC20770A.

[9] P. Hahn, I. Leibacher, T. Baasch, and J. Dual, “Numerical simulation of acoustofluidic manipulation by radiation forces and acoustic streaming for complex particles,” *Lab. Chip*, vol. 15, no. 22, pp. 4302–4313, Oct. 2015, doi: 10.1039/C5LC00866B.

[10] M. S. Namnabat, M. Moghimi Zand, and E. Houshfar, “3D numerical simulation of acoustophoretic motion induced by boundary-driven acoustic streaming in standing

surface acoustic wave microfluidics," *Sci. Rep.*, vol. 11, no. 1, Art. no. 1, Jun. 2021, doi: 10.1038/s41598-021-90825-z.

[11] H. Ahmed *et al.*, "A Pumpless Acoustofluidic Platform for Size-Selective Concentration and Separation of Microparticles," *Anal. Chem.*, vol. 89, no. 24, pp. 13575–13581, Dec. 2017, doi: 10.1021/acs.analchem.7b04014.

[12] M. Settnes and H. Bruus, "Forces acting on a small particle in an acoustical field in a viscous fluid," *Phys. Rev. E*, vol. 85, no. 1, p. 016327, Jan. 2012, doi: 10.1103/PhysRevE.85.016327.

[13] S. B. Borrelle *et al.*, "Predicted growth in plastic waste exceeds efforts to mitigate plastic pollution," *Science*, vol. 369, no. 6510, pp. 1515–1518, Sep. 2020, doi: 10.1126/science.aba3656.

[14] N. B. Hartmann *et al.*, "Are We Speaking the Same Language? Recommendations for a Definition and Categorization Framework for Plastic Debris," *Environ. Sci. Technol.*, vol. 53, no. 3, pp. 1039–1047, Feb. 2019, doi: 10.1021/acs.est.8b05297.

[15] I. E. Napper *et al.*, "The abundance and characteristics of microplastics in surface water in the transboundary Ganges River," *Environ. Pollut. Barking Essex 1987*, vol. 274, p. 116348, Apr. 2021, doi: 10.1016/j.envpol.2020.116348.

[16] L. M. Pinheiro, V. O. Agostini, A. R. A. Lima, R. D. Ward, and G. L. L. Pinho, "The fate of plastic litter within estuarine compartments: An overview of current knowledge for the transboundary issue to guide future assessments," *Environ. Pollut. Barking Essex 1987*, vol. 279, p. 116908, Jun. 2021, doi: 10.1016/j.envpol.2021.116908.

[17] T. R. Walker, "(Micro)plastics and the UN Sustainable Development Goals," *Curr. Opin. Green Sustain. Chem.*, vol. 30, p. 100497, Aug. 2021, doi: 10.1016/j.cogsc.2021.100497.

[18] J. S. Hanvey, P. J. Lewis, J. L. Lavers, N. D. Crosbie, K. Pozo, and B. O. Clarke, "A review of analytical techniques for quantifying microplastics in sediments," *Anal. Methods*, vol. 9, no. 9, pp. 1369–1383, Mar. 2017, doi: 10.1039/C6AY02707E.

[19] H. Bruus *et al.*, "Forthcoming Lab on a Chip tutorial series on acoustofluidics: Acoustofluidics—exploiting ultrasonic standing wave forces and acoustic streaming in microfluidic systems for cell and particle manipulation," *Lab. Chip*, vol. 11, no. 21, pp. 3579–3580, Oct. 2011, doi: 10.1039/C1LC90058G.

[20] H. Bruus, *Theoretical Microfluidics*. 2008.

[21] R. B. Henrik Bruus, “Acoustofluidics: theory and simulation of radiation forces at ultrasound resonances in microfluidic devices,” *Proc. Meet. Acoust.*, vol. 6, Jul. 2009, doi: 10.1121/1.3186746.

[22] H. Bruus, “Acoustofluidics 7: The acoustic radiation force on small particles,” *Lab. Chip*, vol. 12, no. 6, pp. 1014–1021, Feb. 2012, doi: 10.1039/C2LC21068A.

[23] S. S. Sadhal, “Acoustofluidics 13: Analysis of acoustic streaming by perturbation methods,” *Lab. Chip*, vol. 12, no. 13, pp. 2292–2300, Jun. 2012, doi: 10.1039/C2LC40202E.

[24] M. Wiklund, R. Green, and M. Ohlin, “Acoustofluidics 14: Applications of acoustic streaming in microfluidic devices,” *Lab. Chip*, vol. 12, no. 14, pp. 2438–2451, Jun. 2012, doi: 10.1039/C2LC40203C.

[25] S. S. Sadhal, “Acoustofluidics 15: streaming with sound waves interacting with solid particles,” *Lab. Chip*, vol. 12, no. 15, pp. 2600–2611, Jul. 2012, doi: 10.1039/C2LC40243B.

[26] “Acoustic Streaming in a Microchannel Cross Section,” *COMSOL*. https://www.comsol.com/model/acoustic-streaming-in-a-microchannel-cross-section-17087 (accessed May 01, 2023).

[27] “models.aco.saw_gas_sensor.pdf.” Accessed: Apr. 17, 2023. [Online]. Available: https://www.comsol.com/model/download/1073641/models.aco.saw_gas_sensor.pdf

[28] “COMSOL: Multiphysics Software for Optimizing Designs,” *COMSOL*. https://www.comsol.com/ (accessed Apr. 21, 2023).

[29] “Acoustic-Structure Interaction with a Perfectly Matched Layer (PML),” *COMSOL*. https://www.comsol.com/model/acoustic-structure-interaction-with-a-perfectly-matched-layer-pml-23521 (accessed Apr. 19, 2023).

[30] “COMSOL Multiphysics Reference Manual”, [Online]. Available: https://www.comsol.com/

[31] V. K. Ozhigin, R. Ingvaldsen, H. Loeng, V. Boitsov, and A. Karsakov, “Introduction to the Barents Sea,” *Barents Sea Ecosyst. Russ.-Nor. Coop. Sci. Manag.*, pp. 315–328, Jan. 2011.

[32] “ocean-sound.pdf.” Accessed: Apr. 14, 2023. [Online]. Available: https://www.ametsoc.org/index.cfm/ams/education-careers/education-program/k-12-

teachers/project-ocean/training-opportunities/maury-project-peer-led-training/maury-project-peer-training-resources/ocean-sound/

[33] Auld, B. A., *Acoustic fields and waves in solids*, 2nd ed. Krieger, 1990.

[34] R. Lu, Y. Yang, S. Link, and S. Gong, "A1 Resonators in 128° Y-cut Lithium Niobate with Electromechanical Coupling of 46.4%," *J. Microelectromechanical Syst.*, vol. 29, no. 3, pp. 313–319, Jun. 2020, doi: 10.1109/JMEMS.2020.2982775.

[35] "GESAMP_microplastics full study.pdf." Accessed: Apr. 18, 2023. [Online]. Available: https://ec.europa.eu/environment/marine/good-environmental-status/descriptor-10/pdf/GESAMP_microplastics%20full%20study.pdf

[36] "How to Automate Meshing in Frequency Bands for Acoustic Simulations," *COMSOL*. https://www.comsol.com/blogs/how-to-automate-meshing-in-frequency-bands-for-acoustic-simulations/ (accessed May 01, 2023).

List of tables and charts

Appendix

Table App-1 shows the expression that is written for introducing travelling acoustic radiation force (ARF), x and y components, as well as Buoyant and Gravitational Forces in COMSOL. The expression for travelling ARF has been entered to the table of *Variable* in the setting window of *Equation View* node of *Acoustophoretic Radiation Force* interface, see figure App-1(a). The expression for Buoyant and Gravitational Forces are also introduced through *Forces* interface from *Particle Tracing for Fluid Flow (fpt)* physics, see figure App-1(b). Note that gravity force is subtracted from Buoyance force to calculate net force along Y-axis.

Table App-1 expressions for travelling ARF and Buoyant and Gravitational Forces which are introduced to COMSOL for simulating MPs trajectories

Name	Expression	Description
fpt.acof1.Fradx	pi*fpt.rp^3*(−(2/3)*fpt.acof1.kappas*imag(fpt.acof1.f0sl)*fpt.acof1.p*conj(fpt.acof1.p)+fpt.rho*imag(fpt.acof1.1sl)*(abs(fpt.acof1.ux)^2+abs(fpt.acof1.uy)^2))*(fpt.acof1.omega/fpt.c_local)*sin(theta)	ARF x-component (N)
fpt.acof1.Frady	pi*fpt.rp^3*(−(2/3)*fpt.acof1.kappas*imag(fpt.acof1.f0sl)*fpt.acof1.p*conj(fpt.acof1.p)+fpt.rho*imag(fpt.acof1.f1sl)*(abs(fpt.acof1.ux)^2+abs(fpt.acof1.uy)^2))*(fpt.acof1.omega/fpt.c_local)*cos(theta)	ARF y-component (N)
Force	fpt.rho*fpt.Vp*g_const-fpt.rhop*fpt.Vp*g_const	Subtraction of gravity force from Buoyance force

For writing the travelling ARF expression, two built-in mathematical functions of *abs* and *imag* for taking absolute value and imaginary part of a complex value are used.

(a)

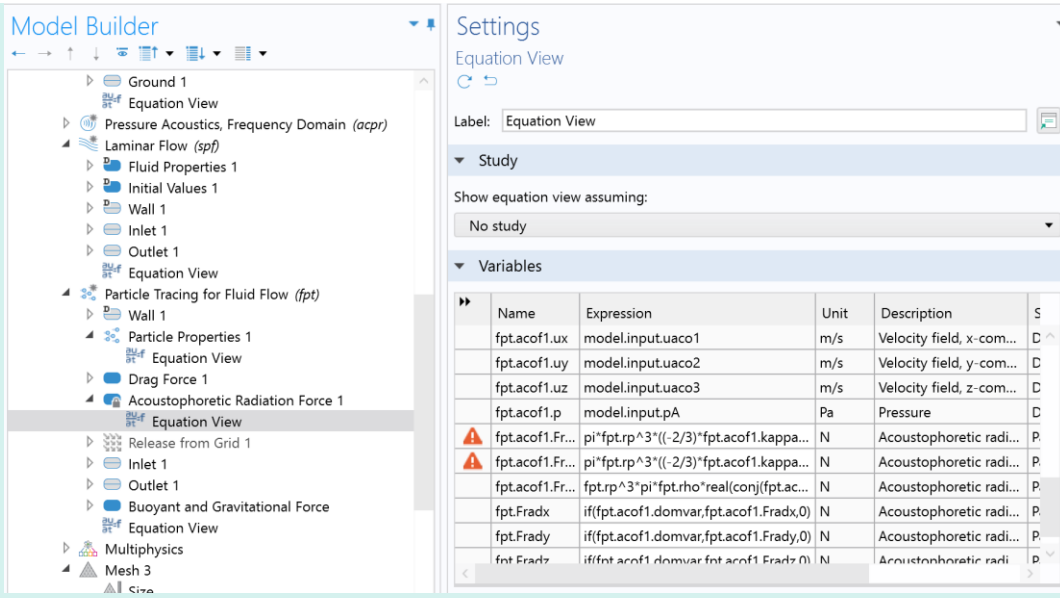

(b)

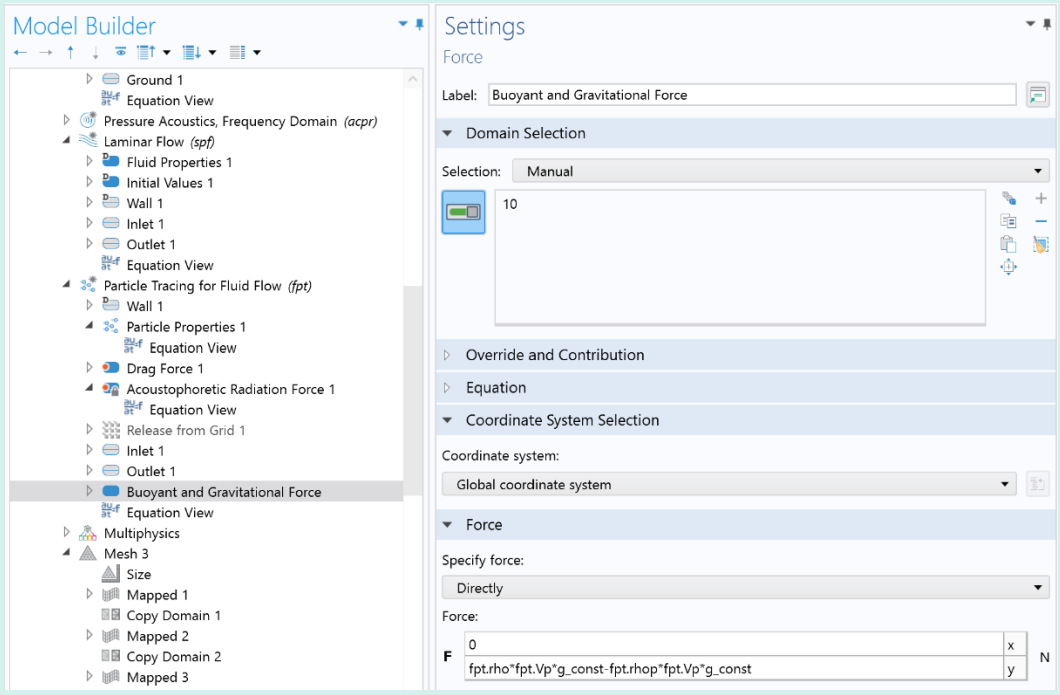

Figure App-1 A screenshot taken from (a) setting window of Equation View node from Acoustophoretic Radiation Force interface and (b) setting window of Buoyant and Gravitational Force

In the expression for travelling ARF, the variable *theta* which is introduced in the *Definitions* interface of COMSOL, is the angle of travelling wave propagation in the fluid relative to Y-axis which has been discussed in chapter 7. Based on the simulation results of acoustic fields and the width of microchannel which is extended from -5855 μm to 6865µm along X-axis, the value of theta for x< 503 μm is -0.4 rad, for x=503 μm is zero and for x> 503 µm is +0.4 rad. This range of theta is expressed in form of if condition:

if(qx<503[um],-0.4[rad],if(qx==503[um],0[rad],0.4[rad]))

where qx is the position of particle on X-axis.

Table App-2 shows a list of variables which are used in the expression of travelling acoustic radiation force [30].

Table App-2 List of some variables used in ARF expression[30]

Name	Expression	Unit	Description
fpt.acof1.omega	2*pi*f0	rad/s	Angular frequency
fpt.c	fpt.c_local	m/s	Fluid sound speed
fpt.rho	fpt.rho_local	kg/m³	Fluid density
fpt.rp	0.5*fpt.dp	m	Particle radius
fpt.Vp	fpt.dp^3*pi/6	m³	Particle volume
fpt.acof1.kappas	1/(fpt.c^2*fpt.rho)	1/Pa	Compressibility (isentropic)
fpt.acof1.f0sl	1-fpt.acof1.kappasp/fpt.acof1.kappas	1	Monopole scattering coefficient of solid particle
fpt.acof1.f1sl	2*(-1+fpt.rhop/fpt.rho)*(1-3*(1/(fpt.acof1.ksf*fpt.rp)-i)/(fpt.acof1.ksf*fpt.rp))/(1+2*fpt.rhop/fpt.rho-9*(1/(fpt.acof1.ksf*fpt.rp)-i)/(fpt.acof1.ksf*fpt.rp))	1	Dipole scattering coefficient of solid particle
fpt.acof1.p	model.input.pA	Pa	Pressure
fpt.acof1.ux	model.input.uaco1	m/s	Velocity field, x-component
fpt.acof1.uy	model.input.uaco2	m/s	Velocity field, y-component